Axial couplings in heavy-hadron chiral perturbation theory at the next-to-leading order

William Detmold,[1,2] C.-J. David Lin,[3,4] and Stefan Meinel[1]

[1]*Department of Physics, College of William and Mary, Williamsburg, Virginia 23187-8795, USA*
[2]*Jefferson Laboratory, 12000 Jefferson Avenue, Newport News, Virginia 23606, USA*
[3]*Institute of Physics, National Chiao-Tung University, Ta-Hsueh Road, Hsinchu 300, Taiwan*
[4]*Division of Physics, National Center for Theoretical Sciences, Kuang-Fu Road, Hsinchu 300, Taiwan*

(Received 6 September 2011; published 9 November 2011)

We present calculations of axial-current matrix elements between various heavy-meson and heavy-baryon states to the next-to-leading order in heavy-hadron chiral perturbation theory in the p-regime. When compared with data from lattice computations or experiments, these results can be used to determine the axial couplings in the chiral Lagrangian. Our calculation is performed in partially quenched chiral perturbation theory for both SU(4|2) and SU(6|3). We incorporate finite-size effects arising from a single Goldstone meson wrapping around the spatial volume. Results for full QCD with two and three flavors can be obtained straightforwardly by taking the sea-quark masses to be equal to the valence-quark masses. To illustrate the impact of our chiral perturbation theory calculation on lattice computations, we analyze the SU(2) full-QCD results in detail. We also study one-loop contributions relevant to the heavy-hadron strong-decay amplitudes involving final-state Goldstone bosons, and demonstrate that the quark-mass dependence of these amplitudes can be significantly different from that of the axial-current matrix elements containing only single-hadron external states.

DOI: 10.1103/PhysRevD.84.094502 PACS numbers: 12.38.Gc, 12.39.Fe, 12.39.Hg, 14.20.Mr

I. INTRODUCTION

The physics of b hadrons is an important and active field of research, both experimentally and theoretically. B mesons have played an important role in our understanding of flavor physics in the standard model (SM) and its possible extension. The ongoing LHCb experiment and possible future B factories will produce significantly improved experimental information for B mesons which will, in turn, lead to better constraints on the relevant SM parameters or reveal deviations from the SM. In addition, a large amount of polarized single-bottom baryon data will be produced. This will allow extensive studies of the spectrum and the decays of these baryons. Since the baryons carry different spin quantum numbers, they may offer additional opportunities for probing the coupling structure of physics beyond the SM. In performing such investigations, it is necessary to compare experimental results to precise theoretical calculations in which nonperturbative strong-interaction effects are well controlled. This is becoming achievable because of the progress in lattice QCD.

Calculations in lattice QCD are often performed at unphysical light-quark masses due to the limited computing resources. In order to obtain high-precision theoretical predictions for spectral quantities and matrix elements, it is essential to use chiral perturbation theory (χPT) to extrapolate to the physical quark masses. For systems of hadrons containing a single valence b or $\bar{b}$ quark, the relevant chiral effective field theory is heavy-hadron χPT (HHχPT) [1–5]. In addition to the low-energy constants in the chiral Lagrangian of the Goldstone boson sector, there are three unknown coupling constants in this effective theory at the leading order (LO). These constants, defined explicitly as $g_{1,2,3}$ in Eq. (24) in Sec. II, accompany axial couplings of heavy hadrons to the Goldstone boson sector and appear in all chiral extrapolations using HHχPT. Therefore, the accurate determination of $g_{1,2,3}$ is one of the most important tasks in the lattice QCD calculations for b-physics phenomenology.

In this work, we compute the matrix elements of the quark-level axial currents,

$$\mathcal{J}_{ud,\mu} = \bar{d}\gamma_\mu\gamma_5 u, \quad \text{and} \quad \mathcal{J}_{us,\mu} = \bar{s}\gamma_\mu\gamma_5 u, \qquad (1)$$

between various heavy-light meson and single-b baryon states to the next-to-leading order (NLO) in HHχPT. In particular, we calculate the relevant one-loop contributions to these matrix elements. When compared with data from lattice calculations or experiments, our results can be used to extract the above-mentioned three axial couplings in HHχPT. Our calculation is performed in partially quenched chiral perturbation theory (PQχPT) using the supersymmetric formulation [6], for both SU(4|2) and SU(6|3). The "full-QCD" limit can be taken straightforwardly from our results by setting the sea-quark masses to be equal to the valence-quark masses. Our one-loop computation is carried out for finite spatial volume in the p-regime,[1] following the same method as in Refs. [9,10]. As pointed out in Ref. [11], in heavy-light meson systems, finite-volume effects arising from higher-order terms in the chiral expansion can be estimated. This requires high-precision information on the $B^* - B - \pi$ coupling beyond that which is currently available. Nevertheless, such

[1]Studies of the heavy-meson systems in the ϵ-regime can be found in Refs. [7,8].

higher-order effects are insignificant for current and future lattice calculations, since computations with small pion masses in large volumes are becoming standard.

In this paper, we present our results in the isospin limit. However, in the case of SU(6|3), we include the SU(3) breaking[2] effects, both in the external states and in the axial currents. At NLO in HHχPT, the axial-current matrix elements for heavy hadrons can be written in the general form

$$g(1 + g^2 L + g'^2 L' + L'') + \text{analytic terms}, \tag{2}$$

where g and g' are variously g_1, g_2, and g_3 in Eq. (24), and L, L', and L'' are the contributions from one-loop diagrams. The determination of g_1 using lattice QCD has been attempted by various groups [12–17]. However, the correct quark-mass dependence (based on the symmetries of QCD) of the axial matrix elements was not previously known. Using the current work, extrapolations to the physical quark masses can be made rigorously.

This paper is organized in the following way. Section II contains an introduction to HHχPT. In Sec. III, we first present the general structure of the one-loop contributions to the axial-current matrix elements, before giving the results in the case of SU(2) in Sec. IV. Results for SU(4|2) and SU(6|3) HHχPT are presented in Sec. V, emphasizing the quark-flavor flow picture. In Sec. VI, the strong-decay amplitudes involving final-state Goldstone mesons are also computed before we conclude. Technical details of the results are included in the Appendices.

II. HEAVY-HADRON CHIRAL PERTURBATION THEORY

The partially quenched (PQ) chiral Lagrangian[3] for the Goldstone mesons is

$$\mathcal{L}_{\mathrm{G}} = \frac{f^2}{8}\mathrm{str}[(\partial_\mu \Sigma^\dagger)(\partial^\mu \Sigma) + \Sigma^\dagger \chi + \chi^\dagger \Sigma] + [\alpha(\partial_\mu \Phi_0)(\partial^\mu \Phi_0) - M_0^2 \Phi_0^2], \tag{3}$$

where $\Sigma = \exp(2i\Phi/f)$ is the nonlinear Goldstone particle field, with Φ being the matrix containing the standard Goldstone fields in the quark-flavor basis. We use $f = 132$ MeV. In this work, we follow the supersymmetric formulation of PQ chiral perturbation theory (PQχPT) [6]. Therefore, under $\mathrm{SU}(4|2)_{\mathrm{L}} \otimes \mathrm{SU}(4|2)_{\mathrm{R}}$ or $\mathrm{SU}(6|3)_{\mathrm{L}} \otimes \mathrm{SU}(6|3)_{\mathrm{R}}$, Σ transforms as

$$\Sigma \to U_{\mathrm{L}} \Sigma U_{\mathrm{R}}^\dagger, \tag{4}$$

where

$$\begin{aligned} U_{\mathrm{L}} &\in \mathrm{SU}(4|2)_{\mathrm{L}} \quad \text{or} \quad \mathrm{SU}(6|3)_{\mathrm{L}}, \\ U_{\mathrm{R}} &\in \mathrm{SU}(4|2)_{\mathrm{R}} \quad \text{or} \quad \mathrm{SU}(6|3)_{\mathrm{R}}. \end{aligned} \tag{5}$$

The symbol "str" in the above equation means "supertrace." The variable χ is defined as

$$\chi \equiv 2B_0 \mathcal{M}_q, \tag{6}$$

where B_0 is a low-energy constant related to the chiral condensate and, in the isospin limit, the quark-mass matrix, $\mathcal{M}_q$ is

$$\mathcal{M}_q = \mathrm{diag}(\underbrace{m_u, m_u}_{\text{valence}}, \underbrace{m_{u'}, m_{u'}}_{\text{sea}}, \underbrace{m_u, m_u}_{\text{ghost}}), \tag{7}$$

in the SU(4|2) theory, and is

$$\mathcal{M}_q = \mathrm{diag}(\underbrace{m_u, m_u, m_s}_{\text{valence}}, \underbrace{m_{u'}, m_{u'}, m_{s'}}_{\text{sea}}, \underbrace{m_u, m_u, m_s}_{\text{ghost}}), \tag{8}$$

in the SU(6|3) theory. We keep the strange quark mass different from that of the up and down quarks in the valence, sea, and ghost sectors. Notice that the flavor-singlet state $\Phi_0 = \mathrm{str}(\Phi)/\sqrt{6}$ is rendered heavy by the $\mathrm{U}(1)_A$ anomaly in PQQCD [19,20] and can be integrated out, resulting in residual "hairpin" structures.

The inclusion of the heavy-light mesons in chiral perturbation theory was first proposed in Refs. [1–3], with the generalization to quenched and partially quenched theories given in Refs. [21,22]. The $1/M_P$ and chiral corrections were studied by Boyd and Grinstein [23]. The B and B^* meson fields appear in this effective theory through the "superfield"

$$H_i^{(\bar{b})} = (B_{i,\mu}^* \gamma^\mu - B_i \gamma_5)\frac{1 - \not{v}}{2}, \tag{9}$$

where v_μ is the 4-velocity of the meson fields, B_i and $B_{i,\mu}^*$ annihilate pseudoscalar and vector mesons containing an anti-b quark[4] and a light quark of flavor i. Under the heavy-quark spin transformation S_h and the unbroken light-flavor transformation $U(x)$, the field $H^{(\bar{b})}$ transforms as

$$H_i^{(\bar{b})}(x) \to U_i{}^j(x) H_j^{(\bar{b})}(x) S_h^{-1}. \tag{10}$$

Also, the conjugate field, which creates heavy-light mesons containing an anti-b quark and a light quark of flavor i, is defined as

$$\bar{H}_i^{(\bar{b})} = \gamma^0 H_i^{(\bar{b})\dagger} \gamma_0, \tag{11}$$

and transforms under S_h and $U(x)$ as

$$\bar{H}_i^{(\bar{b})}(x) \to S_h \bar{H}_j^{(\bar{b})}(x)(U^\dagger)^j{}_i(x). \tag{12}$$

[2]More precisely, we consider identical SU(3) breaking effects in the sea, valence, and ghost sectors of SU(6|3) but for simplicity, refer to this as SU(3) breaking.

[3]In this paper, we only address situations where there are no multiparticle thresholds involved in loops. Therefore, in spite of the sickness pointed out in Ref. [18], we can still use the Minkowski formalism of PQ chiral perturbation theory.

[4]We follow the standard notation [24] for the flavor content of B mesons, so that e.g. $B_u = B^+ = u\bar{b}$.

The introduction of the single-b baryons to χPT was pioneered by authors of Refs. [3–5], and the effective theory was generalized to the PQ scenario in Ref. [25]. Since the two valence light quarks in such baryons may carry total spin quantum numbers[5] $s_l = 0$ or $s_l = 1$, there are two types of heavy baryons. At the quark level, these two types of baryons carrying light flavors i and j are described by the interpolating fields

$$\begin{aligned}\mathcal{T}^{\gamma}_{ij} &\sim b^{\gamma,c}[q_i^{\alpha,a}q_j^{\beta,b} + q_j^{\beta,b}q_i^{\alpha,a}]\epsilon_{abc}(C\gamma_5)_{\alpha\beta} \quad \text{for } s_l = 0,\\ \mathcal{S}^{\gamma,\mu}_{ij} &\sim b^{\gamma,c}[q_i^{\alpha,a}q_j^{\beta,b} - q_j^{\beta,b}q_i^{\alpha,a}]\epsilon_{abc}(C\gamma^{\mu})_{\alpha\beta} \quad \text{for } s_l = 1,\end{aligned} \tag{13}$$

where C is the charge-conjugation matrix, α, β, and γ are the Dirac indices, and a, b, and c are color indices. In full QCD, the $\mathcal{T}$ fields are antisymmetric and the $\mathcal{S}$ fields are symmetric under the exchange of the light-flavor indices. In the PQ theory, the flavor structure of these interpolating fields has the properties

$$\mathcal{T}_{ij} = (-1)^{\eta_i\eta_j}\mathcal{T}_{ji}, \qquad \mathcal{S}^{\mu}_{ij} = (-1)^{1+\eta_i\eta_j}\mathcal{S}^{\mu}_{ji}, \tag{14}$$

where

$$\eta_i = \begin{cases} 1 \text{ when } i \in \text{valence and sea,} \\ 0 \text{ when } i \in \text{ghost,}\end{cases} \tag{15}$$

accounts for different statistics of quarks in PQQCD. These fields transform as **39**- and **42**-plets under the SU(6|3) flavor rotation, while they transform as **17**- and **19**-plets under the SU(4|2) flavor rotation. The baryon fields are included in heavy-hadron chiral perturbation theory (HHχPT) according to the flavor properties in Eq. (14). In the case of $N_f = 3$ (N_f refers to the number of sea-quark flavors), the pure valence-valence sector of the $s_l = 0$ baryons is related to the physical states of Λ_b and $\Xi_b^{\pm 1/2}$ via

$$T_{(\text{valence-valence})} = \frac{1}{\sqrt{2}}\begin{pmatrix} 0 & \Lambda_b & \Xi_b^{+1/2} \\ -\Lambda_b & 0 & \Xi_b^{-1/2} \\ -\Xi_b^{+1/2} & -\Xi_b^{-1/2} & 0 \end{pmatrix}, \tag{16}$$

where the superscript indicates the 3-component of the isospin. Since the light-light diquark is of spin-1 in the $\mathcal{S}^{\mu}_{ij}$ fields, such baryons can be in spin $1/2$ or $3/2$ states which are degenerate in the heavy-quark limit. Therefore, they are best described by the superfield

$$S^{\mu}_{ij} = \sqrt{\frac{1}{3}}(v^{\mu} + \gamma^{\mu})\gamma_5 B_{ij} + B^{*\mu}_{ij}, \tag{17}$$

where B_{ij} and $B^{*\mu}_{ij}$ are spin-$1/2$ and $3/2$ baryons. In the pure valence-valence sector,

$$B_{(\text{valence-valence})} = \begin{pmatrix} \Sigma_b^{+1} & \frac{1}{\sqrt{2}}\Sigma_b^0 & \frac{1}{\sqrt{2}}\Xi_b^{\prime+1/2} \\ \frac{1}{\sqrt{2}}\Sigma_b^0 & \Sigma_b^{-1} & \frac{1}{\sqrt{2}}\Xi_b^{\prime-1/2} \\ \frac{1}{\sqrt{2}}\Xi_b^{\prime+1/2} & \frac{1}{\sqrt{2}}\Sigma_b^0 & \Omega_b \end{pmatrix}, \tag{18}$$

and similarly for the $B^{*\mu}_{ij}$ fields. The S^{μ}_{ij} and T_{ij} fields have the same property as $\bar{H}_i^{(\bar{b})}$ under the heavy-quark spin transformation S_h. For the unbroken light-flavor transformation,

$$\begin{aligned}S^{\mu}_{ij}(x) &\to U_i{}^k(x)U_j{}^l(x)S^{\mu}_{kl}(x),\\ T_{ij}(x) &\to U_i{}^k(x)U_j{}^l(x)T_{kl}(x),\end{aligned} \tag{19}$$

with the flavor indices satisfying Eq. (14). These S^{μ}_{ij} and T_{ij} are annihilation field operators and we denote the corresponding creation fields by $\bar{S}^{\mu}_{ij}$ and $\bar{T}_{ij}$.

The Goldstone mesons couple to the above heavy-meson and baryon fields in the HHχPT Lagrangian via the nonlinear realization

$$\xi \equiv e^{i\Phi/f} = \sqrt{\Sigma}, \tag{20}$$

which transforms as

$$\xi(x) \to U_L\xi(x)U^{\dagger}(x) = U(x)\xi(x)U_R^{\dagger}. \tag{21}$$

The ξ field can be used to construct vector and axial-vector fields

$$V^{\mu} = \frac{1}{2}(\xi^{\dagger}\partial^{\mu}\xi + \xi\partial^{\mu}\xi^{\dagger}), \quad A^{\mu} = \frac{i}{2}(\xi^{\dagger}\partial^{\mu}\xi - \xi\partial^{\mu}\xi^{\dagger}). \tag{22}$$

The vector field can then serve as the gauge field in defining the chiral covariant derivative which acts on the heavy hadrons,

$$\begin{aligned}\mathcal{D}^{\mu}H_i^{(\bar{b})} &= \partial^{\mu}H_i^{(\bar{b})} + (V^{\mu})_i{}^j H_j^{(\bar{b})},\\ \mathcal{D}^{\mu}T_{ij} &= \partial^{\mu}T_{ij} + (V^{\mu})_i{}^k T_{kj} + (-1)^{\eta_i(\eta_j+\eta_k)}(V^{\mu})_j{}^k T_{ik},\\ \mathcal{D}^{\mu}S^{\nu}_{ij} &= \partial^{\mu}S^{\nu}_{ij} + (V^{\mu})_i{}^k S^{\nu}_{kj} + (-1)^{\eta_i(\eta_j+\eta_k)}(V^{\mu})_j{}^k S^{\nu}_{ik}.\end{aligned} \tag{23}$$

The leading-order HHχPT Lagrangian is then

$$\begin{aligned}\mathcal{L}^{(\text{LO})}_{\text{HH}\chi\text{PT}} = &-i\text{tr}_D[\bar{H}^{(\bar{b})i}v_{\mu}\mathcal{D}^{\mu}H_i^{(\bar{b})}] + i(\bar{T}v_{\mu}\mathcal{D}^{\mu}T)_{\text{f}}\\ &- i(\bar{S}^{\nu}v_{\mu}\mathcal{D}^{\mu}S_{\nu})_{\text{f}} + \Delta^{(B)}(\bar{S}^{\nu}S_{\nu})_{\text{f}}\\ &+ g_1\text{tr}_D[\bar{H}_i^{(\bar{b})}\gamma^{\mu}\gamma_5 H_j^{(\bar{b})}A^{ij}_{\mu}]\\ &- ig_2\epsilon_{\mu\nu\sigma\rho}(\bar{S}^{\mu}v^{\nu}A^{\sigma}S^{\rho})_{\text{f}}\\ &+ \sqrt{2}g_3[(\bar{T}A^{\mu}S_{\mu})_{\text{f}} + (\bar{S}_{\mu}A^{\mu}T)_{\text{f}}],\end{aligned} \tag{24}$$

where v_{μ} is the velocity of the heavy hadrons, $\text{tr}_D[\,]$ means taking the trace in Dirac space, and $(\,)_{\text{f}}$ is the implementation of the PQ-theory flavor contraction rules [25]

[5]The total spin of the light degrees of freedom is a conserved quantum number because of the heavy-quark symmetry.

$$(\bar{T}YT)_{\rm f} = \bar{T}^{ji} Y_i{}^l T_{lj}, \qquad (\bar{S}^\mu Y S_\mu)_{\rm f} = \bar{S}^{\mu,ji} Y_i{}^l S_{\mu,lj},$$
$$(\bar{T}Y^\mu S_\mu)_{\rm f} = \bar{T}^{ji} (Y^\mu)_i{}^l S_{\mu,lj}. \tag{25}$$

The parameter $\Delta^{(B)}$ is the mass difference between the S and T fields with the same light-flavor indices,

$$\Delta^{(B)} = M_{S_{i,j}} - M_{T_{i,j}}.$$

It is grouped together with the definition of other mass parameters in Eq. (A1) in Appendix A. This mass difference is of $O(\Lambda_{\rm QCD})$, and does not vanish either in the chiral limit or in the heavy-quark limit.

The LO Lagrangian for HHχPT contains terms of $O(p)$ and no light-quark-mass dependence. To generate the flavor SU(3) breaking effects in heavy-meson and baryon spectrum, which give rise to the mass differences $\delta^{(M)}_{i,j}$ and $\delta^{(B)}_{ij,kl}$ in Eq. (A1), one introduces

$$\begin{aligned}\mathcal{L}^{(\chi)}_{\rm HH\chi PT} = {} & \lambda_1 {\rm tr}_{\rm D}[\bar{H}^{(\bar{b})}_i \chi^{ij}_\xi H^{(\bar{b})}_j] + \lambda_2 {\rm tr}_{\rm D}[\bar{H}^{(\bar{b})i} H^{(\bar{b})}_i] {\rm str}(\chi_\xi) \\ & + \lambda_3 (\bar{S}^\mu \chi_\xi S_\mu)_{\rm f} + \lambda_4 (\bar{S}^\mu S_\mu)_{\rm f} {\rm str}(\chi_\xi) \\ & + \lambda_5 (\bar{T}\chi_\xi T)_{\rm f} + \lambda_6 (\bar{T}T)_{\rm f} {\rm str}(\chi_\xi),\end{aligned} \tag{26}$$

where

$$\chi_\xi = \xi\chi\xi + \xi^\dagger\chi\xi^\dagger. \tag{27}$$

In the computation of the axial-current matrix elements, the flavor breaking effects in Eq. (26) are formally subleading compared to those encoded in the pure Goldstone Lagrangian, Eq. (3). Nevertheless, we keep them in our calculation as they can be numerically significant.

In this work, we also include the heavy-quark spin symmetry breaking term

$$\frac{\bar{\lambda}_2}{M_B} {\rm tr}_{\rm D}[\bar{H}^{(\bar{b})i} \sigma_{\mu\nu} H^{(\bar{b})}_i \sigma^{\mu\nu}], \tag{28}$$

where M_B is the B meson mass. This counterterm leads to the mass difference between the B^* and B mesons with the same light flavor,

$$\Delta^{(M)} = M_{B^*_i} - M_{B_i},$$

which vanishes in the heavy-quark limit. This mass difference is also grouped together with other mass parameters in Eq. (A1) in Appendix A. In principle, there are also such heavy-quark spin breaking terms in the baryon sector, resulting in mass differences between B_{ij} and B^*_{ij} baryons in Eq. (17). However, these mass differences are numerically much smaller than $\Delta^{(M)}$ [26].

III. AXIAL-CURRENT MATRIX ELEMENTS AT THE NEXT-TO-LEADING ORDER

Applying the Noether theorem to the chiral Lagrangian in the previous section, one can derive the leading-order axial currents corresponding to their quark-level counterparts in Eq. (1). For matrix elements involving external states of single heavy hadrons, the relevant LO currents are

$$\begin{aligned}J^{(N_f)}_{ij,\mu} = {} & g_1 {\rm tr}_{\rm D}[\bar{H}^{(\bar{b})}_k \gamma_\mu \gamma_5 H^{(\bar{b})}_l (\tau^{(+)}_{ij,\xi})^{kl}] \\ & - i g_2 \epsilon_{\mu\nu\sigma\rho} (\bar{S}^\nu v^\sigma \tau^{(+)}_{ij,\xi} S^\rho)_{\rm f} + \sqrt{2} g_3 [(\bar{S}_\mu \tau^{(+)}_{ij,\xi} T)_{\rm f} \\ & + (\bar{T}\tau^{(+)}_{ij,\xi} S_\mu)_{\rm f}],\end{aligned} \tag{29}$$

where the subscript ij means the current changes the light-quark flavors from i to j, and

$$\tau^{(+)}_{ij,\xi} = \tfrac{1}{2}(\xi^\dagger \tau_{ij} \xi + \xi \tau_{ij} \xi^\dagger), \tag{30}$$

with the matrices τ_{ij} defined as

$$(\tau_{ij})_{kl} = \delta_{il}\delta_{jk}, \tag{31}$$

where k and l run through all the light-quark flavors in PQQCD. The superscript N_f is the number of sea-quark flavors and $N_f = 2, 3$ represent the cases of SU(4|2) and SU(6|3), respectively. These leading-order axial currents generate the LO terms, as well as the NLO contributions via one-loop corrections, in the matrix elements studied in this work.[6]

There is a significant increase in the number of terms in the next-to-leading-order axial currents in HHχPT, and we postpone the detailed investigation of these NLO currents to Sec. III B below. Here, we first write down the generic form of the chiral expansion of the axial-current matrix elements to the NLO,

$$\begin{aligned}&\langle H_j | \mathcal{J}_{ij,\mu} | H_i \rangle_{\rm QCD} \\ &= \langle H_j | J^{(N_f)}_{ij,\mu} | H_i \rangle_{\rm LO} \times \Big[1 + \frac{1}{f^2} (\mathcal{T}^{(N_f)}_{ij} + \mathcal{W}^{(N_f)}_{H_i} + \mathcal{W}^{(N_f)}_{H_j} \\ &\quad + \mathcal{Q}^{(N_f)}_{H_i \to H_j}) + \mathcal{N}^{(N_f)}_{H_i \to H_j} \Big],\end{aligned} \tag{32}$$

where the equality symbol means the matching between (PQ)QCD and the chiral effective theory, μ is the Lorentz index, and $\mathcal{J}_{ij,\mu}$ are the quark-level currents given in Eq. (1). The flavor indices are denoted by i and j which are *not* summed in the above expression, and H_i is a heavy-hadron state (meson or baryon) containing the light flavor i. The symbols $\mathcal{T}^{(N_f)}_{ij}$, $\mathcal{W}^{(N_f)}_{H_i}$, and $\mathcal{Q}^{(N_f)}_{H_i \to H_j}$ are results from the tadpole, wave-function renormalization, and sunset diagrams at one-loop, as depicted in Fig. 1, where single and double solid lines represent generically the external and internal heavy hadrons while the dashed lines are the Goldstone propagators. The circled crosses in Fig. 1 are the insertions of the LO axial current $J^{(N_f)}_{ij,\mu}$ given in Eq. (29). The tadpole contributions $\mathcal{T}^{(N_f)}_{ij}$ are indepen-

[6] In addition to the terms in Eq. (29), there are other operators in the LO currents arising from the chiral Lagrangian introduced in the previous section. Nevertheless, these terms do not appear in the matrix elements to the order we work at. That is, their contributions to the one-loop corrections vanish.

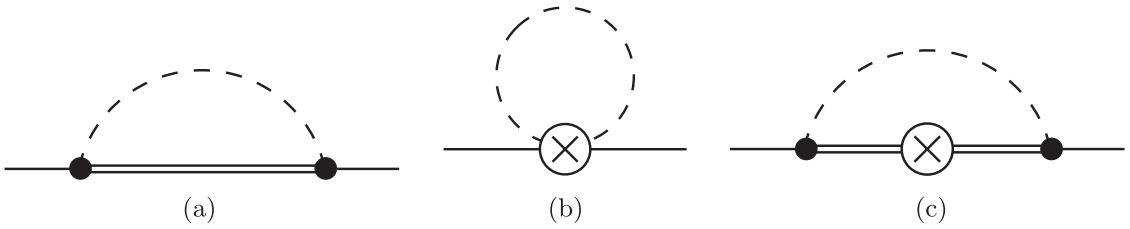

FIG. 1. One-loop diagrams contributing to the matrix elements of axial currents between heavy hadrons. The dashed lines are the Goldstone meson propagators, including the possible hairpin structures. The single solid lines denote generically the external heavy hadrons, while the double solid lines are the internal heavy hadrons. They can be B, B^* mesons or T_{ij}, S_{ij} baryons. The circled crosses are the insertions of the LO axial-current $J^{(N_f)}_{ij,\mu}$ given in Eq. (29), while the other vertices are from the strong chiral Lagrangian in Eq. (24). Diagram (a) is the self-energy of the heavy hadron and it leads to the wave-function renormalization contribution to the matrix elements. Diagrams (b) and (c) are the "tadpole" and "sunset" types, respectively.

dent of the external states, since they emerge completely from the flavor structure of the currents.

In Eq. (32), we have written the NLO analytic terms as the LO matrix elements times $\mathcal{N}^{(N_f)}_{H_i\to H_j}$. In Sec. III B below, we will study these NLO analytic terms, and show that they can be presented in this manner. In this section, we examine the analytic terms (polynomials in the Goldstone masses) in the matrix elements in Eq. (32) for various external states. These are encoded in

$$\langle H_j|J^{(N_f)}_{ij,\mu}|H_i\rangle_{\rm LO} \quad \text{and} \quad \mathcal{N}^{(N_f)}_{H_i\to H_j}.$$

The nonanalytic contributions arising from the one-loop diagrams will be discussed in Secs. IV and V.

A. Leading-order matrix elements

Lattice computations are often performed using the baryon interpolating fields in Eq. (13). Therefore, we carry out the χPT calculation for the T_{ij} and S^μ_{ij} external states. From our results, it is straightforward to obtain matrix elements for physical external baryon states using Eqs. (16) and (18). The leading-order HHχPT predictions for the matrix elements studied in this work are

$$\begin{aligned}
\langle B^*_d|J^{(N_f)}_{ud,\mu}|B_u\rangle_{\rm LO} &= \langle B^*_s|J^{(3)}_{us,\mu}|B_u\rangle_{\rm LO} \quad = -2g_1\varepsilon^*_\mu,\\
\langle S_{dd}|J^{(N_f)}_{ud,\mu}|T_{du}\rangle_{\rm LO} &= \sqrt{2}\langle S_{sd}|J^{(3)}_{ud,\mu}|T_{su}\rangle_{\rm LO}\\
&= \sqrt{2}\langle S_{ds}|J^{(3)}_{us,\mu}|T_{du}\rangle_{\rm LO}\\
&= \langle S_{ss}|J^{(3)}_{us,\mu}|T_{su}\rangle_{\rm LO}\\
&= -g_3\bar{U}_\mu\mathcal{U},\\
\langle S_{dd}|J^{(N_f)}_{ud,\mu}|S_{du}\rangle_{\rm LO} &= \sqrt{2}\langle S_{sd}|J^{(3)}_{ud,\mu}|S_{su}\rangle_{\rm LO}\\
&= \sqrt{2}\langle S_{ds}|J^{(3)}_{us,\mu}|S_{du}\rangle_{\rm LO}\\
&= \langle S_{ss}|J^{(3)}_{us,\mu}|S_{su}\rangle_{\rm LO}\\
&= -\frac{i}{\sqrt{2}}g_2 v^\sigma\epsilon_{\sigma\mu\nu\rho}\bar{U}^\nu U^\rho,
\end{aligned} \tag{33}$$

where ε^μ is the polarization vector of the B^* meson, $\mathcal{U}$ is the Dirac spinor of the T baryon, and the U^μ's are the "superfield spinors" of the S baryons. The basis polarization vectors and spinors satisfy the spin sums

$$\begin{aligned}
\sum_{s=1}^{3}\varepsilon_\mu(v,s)\varepsilon^*_\nu(v,s) &= -g_{\mu\nu}+v_\mu v_\nu,\\
\sum_{s=1}^{2}\mathcal{U}(v,s)\bar{\mathcal{U}}(v,s) &= \frac{1+\not{v}}{2},\\
\sum_{s=1}^{6}U^\mu(v,s)\bar{U}^\nu(v,s) &= -(g^{\mu\nu}-v^\mu v^\nu)\frac{1+\not{v}}{2}.
\end{aligned} \tag{34}$$

Note that U^μ is not a Rarita-Schwinger spinor; instead it contains the degrees of freedom of both the spin-1/2 and spin-3/2 components of the superfield. In Eq. (33), the states are normalized as

$$\begin{aligned}
\langle B_i(v,\mathbf{k})|B_i(v,\mathbf{k}')\rangle &= 2v^0(2\pi)^3\delta^3(\mathbf{k}-\mathbf{k}'),\\
\langle B^*_i(v,\mathbf{k},s)|B^*_i(v,\mathbf{k}',s')\rangle &= 2v^0(2\pi)^3\delta_{ss'}\delta^3(\mathbf{k}-\mathbf{k}'),\\
\langle T_{ij}(v,\mathbf{k},s)|T_{ij}(v,\mathbf{k}',s')\rangle &= v^0(2\pi)^3\delta_{ss'}\delta^3(\mathbf{k}-\mathbf{k}'),\\
\langle S_{ij}(v,\mathbf{k},s)|S_{ij}(v,\mathbf{k}',s')\rangle &= v^0(2\pi)^3\delta_{ss'}\delta^3(\mathbf{k}-\mathbf{k}').
\end{aligned} \tag{35}$$

B. Next-to-leading-order analytic terms

In this subsection, we investigate the NLO counterterms in the axial currents. Their matrix elements between single heavy-hadron states are written as

$$\langle H_j|J^{(N_f)}_{ij,\mu}|H_i\rangle_{\rm LO}\times\mathcal{N}^{(N_f)}_{H_i\to H_j},$$

in Eq. (32). These NLO counterterms play a significant role in the chiral expansion, since they have to be included to renormalize the one-loop contributions from the LO axial currents to matrix elements.

First, we notice that the chiral Lagrangian in Eq. (26) does not contain any space-time derivative, therefore it does not lead to new terms in the axial currents upon applying the Noether theorem. To obtain the NLO axial currents, we introduce additional operators in the chiral Lagrangian,

$$\begin{aligned}\mathcal{L}^{(\mathrm{NLO,axial})}_{\mathrm{HH}\chi\mathrm{PT}} &= \kappa_1^{(H)}\mathrm{tr}_{\mathrm{D}}[\bar{H}_i^{(\bar{b})}\gamma^\mu\gamma_5 H_j^{(\bar{b})}(A_\mu)^i{}_k\chi_\xi^{kj}] + \kappa_2^{(H)}\mathrm{tr}_{\mathrm{D}}[\bar{H}_i^{(\bar{b})}\gamma^\mu\gamma_5 H_j^{(\bar{b})}\chi_\xi^{ik}(A_\mu)_k{}^j] + \kappa_3^{(H)}\mathrm{tr}_{\mathrm{D}}[\bar{H}_i^{(\bar{b})}\gamma^\mu\gamma_5 H_j^{(\bar{b})}(A_\mu)^{ij}]\mathrm{str}(\chi_\xi)\\ &+ \kappa_4^{(H)}\mathrm{tr}_{\mathrm{D}}[\bar{H}_i^{(\bar{b})}\gamma^\mu\gamma_5 H_i^{(\bar{b})}(A_\mu)_{kl}\chi_\xi^{lk}] + \kappa_1^{(S)}\epsilon_{\mu\nu\sigma\rho}(\bar{S}^\mu v^\nu A^\sigma\chi_\xi S^\rho)_{\mathrm{f}} + \kappa_2^{(S)}\epsilon_{\mu\nu\sigma\rho}(\bar{S}^\mu v^\nu\chi_\xi A^\sigma S^\rho)_{\mathrm{f}}\\ &+ \kappa_3^{(S)}\epsilon_{\mu\nu\sigma\rho}(\bar{S}^\mu v^\nu A^\sigma S^\rho)_{\mathrm{f}}\mathrm{str}(\chi_\xi) + \kappa_4^{(S)}\epsilon_{\mu\nu\sigma\rho}(\bar{S}^\mu v^\nu S^\rho)_{\mathrm{f}}\mathrm{str}(A^\sigma\chi_\xi) + \kappa_1^{(T)}[(\bar{T}A^\mu\chi_\xi S_\mu)_{\mathrm{f}}\\ &+ (\bar{S}_\mu A^\mu\chi_\xi T)_{\mathrm{f}}] + \kappa_2^{(T)}[(\bar{T}\chi_\xi A^\mu S_\mu)_{\mathrm{f}} + (\bar{S}_\mu\chi_\xi A^\mu T)_{\mathrm{f}}] + \kappa_3^{(T)}[(\bar{T}A^\mu S_\mu)_{\mathrm{f}} + (\bar{S}_\mu A^\mu T)_{\mathrm{f}}]\mathrm{str}(\chi_\xi), \end{aligned} \tag{36}$$

where χ_ξ is defined in Eq. (27). The mesonic sector of the above Lagrangian was already introduced in Refs. [23,27]. Upon applying the Noether theorem to Eq. (36), one obtains the currents which lead to the NLO analytic terms $\mathcal{N}^{(N_f)}_{H_i\to H_j}$ in Eq. (32),

$$\begin{aligned}J^{(\mathrm{NLO,analytic})}_{ij,\mu} &= \kappa_1^{(H)}\mathrm{tr}_{\mathrm{D}}[\bar{H}_k^{(\bar{b})}\gamma_\mu\gamma_5 H_l^{(\bar{b})}(\tau^{(+)}_{ij,\xi}\chi_\xi)^{kl}] + \kappa_2^{(H)}\mathrm{tr}_{\mathrm{D}}[\bar{H}_k^{(\bar{b})}\gamma_\mu\gamma_5 H_l^{(\bar{b})}(\chi_\xi\tau^{(+)}_{ij,\xi})^{kl}] + \kappa_3^{(H)}\mathrm{tr}_{\mathrm{D}}[\bar{H}_k^{(\bar{b})}\gamma_\mu\gamma_5 H_l^{(\bar{b})}(\tau^{(+)}_{ij,\xi})^{kl}]\mathrm{str}(\chi_\xi)\\ &+ \kappa_4^{(H)}\mathrm{tr}_{\mathrm{D}}[\bar{H}_k^{(\bar{b})}\gamma_\mu\gamma_5 H_k^{(\bar{b})}(\tau^{(+)}_{ij,\xi}\chi_\xi)^{ll}] + \kappa_1^{(S)}\epsilon_{\mu\nu\sigma\rho}(\bar{S}^\nu v^\sigma\tau^{(+)}_{ij,\xi}\chi_\xi S^\rho)_{\mathrm{f}} + \kappa_2^{(S)}\epsilon_{\mu\nu\sigma\rho}(\bar{S}^\nu v^\sigma\chi_\xi\tau^{(+)}_{ij,\xi}S^\rho)_{\mathrm{f}}\\ &+ \kappa_3^{(S)}\epsilon_{\mu\nu\sigma\rho}(\bar{S}^\nu v^\sigma\tau^{(+)}_{ij,\xi}S^\rho)_{\mathrm{f}}\mathrm{str}(\chi_\xi) + \kappa_4^{(S)}\epsilon_{\mu\nu\sigma\rho}(\bar{S}^\nu v^\sigma S^\rho)_{\mathrm{f}}\mathrm{str}(\tau^{(+)}_{ij,\xi}\chi_\xi) + \kappa_1^{(T)}[(\bar{T}\tau^{(+)}_{ij,\xi}\chi_\xi S_\mu)_{\mathrm{f}} + (\bar{S}_\mu\tau^{(+)}_{ij,\xi}\chi_\xi T)_{\mathrm{f}}]\\ &+ \kappa_2^{(T)}[(\bar{T}\chi_\xi\tau^{(+)}_{ij,\xi}S_\mu)_{\mathrm{f}} + (\bar{S}_\mu\chi_\xi\tau^{(+)}_{ij,\xi}T)_{\mathrm{f}}] + \kappa_3^{(T)}[(\bar{T}\tau^{(+)}_{ij,\xi}S_\mu)_{\mathrm{f}} + (\bar{S}_\mu\tau^{(+)}_{ij,\xi}T)_{\mathrm{f}}]\mathrm{str}(\chi_\xi), \end{aligned} \tag{37}$$

where $\tau^{(+)}_{ij,\xi}$ is defined in Eq. (30). Although it is not explicitly shown in the above equation, these NLO currents depend on N_f.

Comparing the currents $J^{(\mathrm{NLO,analytic})}_{ij,\mu}$ to their leading-order counterparts, $J^{(N_f)}_{ij,\mu}$ in Eq. (29), one observes that they share the similar feature in the combination of the heavy-hadron fields with the flavor matrices $\tau^{(+)}_{ij,\xi}$. The complication in $J^{(\mathrm{NLO,analytic})}_{ij,\mu}$ results completely from the insertion of χ_ξ, which contains one power of the quark-mass matrix. This shows that one can write the NLO matrix elements as

$$\langle H_j|J^{(\mathrm{NLO,analytic})}_{ij,\mu}|H_i\rangle_{\mathrm{NLO}} = \langle H_j|J^{(N_f)}_{ij,\mu}|H_i\rangle_{\mathrm{LO}}\times\mathcal{N}^{(N_f)}_{H_i\to H_j},$$

and

$$\mathcal{N}^{(N_f)}_{H_i\to H_j} \sim O(m_q) \sim O(M^2_{\mathrm{Goldstone}}),$$

where m_q is the light-quark mass.

IV. ONE-LOOP CONTRIBUTIONS IN SU(2) HHχPT

We now turn to the discussion of the one-loop results for the axial-current matrix elements. In this section, we first present a simple case, namely, SU(2) χPT in the infinite-volume limit, and use it to illustrate the main features of these one-loop contributions. Details of the SU(4|2) and SU(6|3) PQχPT results are addressed in the next section.

We start by reducing the leading-order matrix elements in Eq. (33) to a simpler form. Notice that all these matrix elements are proportional to the axial couplings, $g_{1,2,3}$. Therefore, from the generic form of the chiral expansion for the axial-current matrix elements given in Eq. (32), we can define the "effective" axial couplings

$$\begin{aligned}(g_1)_{\mathrm{eff}} &= g_1\times\Big[1+\frac{1}{f^2}(\mathcal{T}^{(2)}_{ud}+\mathcal{W}^{(2)}_{B_u}+\mathcal{W}^{(2)}_{B_d^*}+\mathcal{Q}^{(2)}_{B_u\to B_d^*})\\ &\quad+\mathcal{N}^{(2)}_{B_u\to B_d^*}\Big],\\ (g_2)_{\mathrm{eff}} &= g_2\times\Big[1+\frac{1}{f^2}(\mathcal{T}^{(2)}_{ud}+\mathcal{W}^{(2)}_{T_{du}}+\mathcal{W}^{(2)}_{S_{dd}}+\mathcal{Q}^{(2)}_{T_{du}\to S_{dd}})\\ &\quad+\mathcal{N}^{(2)}_{T_{du}\to S_{dd}}\Big],\\ (g_3)_{\mathrm{eff}} &= g_3\times\Big[1+\frac{1}{f^2}(\mathcal{T}^{(2)}_{ud}+\mathcal{W}^{(2)}_{S_{du}}+\mathcal{W}^{(2)}_{S_{dd}}+\mathcal{Q}^{(2)}_{S_{du}\to S_{dd}})\\ &\quad+\mathcal{N}^{(2)}_{S_{du}\to S_{dd}}\Big], \end{aligned} \tag{38}$$

with the wave-function renormalization ($\mathcal{W}$), tadpole ($\mathcal{T}$), and sunset ($\mathcal{Q}$) diagram contributions from Figs. 1(a)–1(c).

The result for the tadpole diagram is particularly simple. In the infinite-volume limit, it is

$$\mathcal{T}^{(2)}_{ud}\overset{\text{infinite-}V}{\longrightarrow} - 2I(M_\pi) = -\frac{2}{16\pi^2}M_\pi^2\log\Big(\frac{M_\pi^2}{\mu^2}\Big),$$

following the definition of the function $I(m)$ in Eq. (B4) in Appendix B. Here, M_π is the pion mass, and μ is the renormalization scale. The dependence on μ is cancelled by the NLO counterterm contributions $\mathcal{N}^{(2)}$ in the above expression for the effective axial couplings.

In this SU(2) full-QCD case, the infinite-volume limit of the wave-function renormalization and sunset diagrams can be written in two functions

$$\begin{aligned}H(m,\Delta) &= \frac{\partial F(m,\Delta)}{\partial\Delta},\\ K(m,\Delta_1,\Delta_2) &= \frac{F(m,\Delta_1)-F(m,\Delta_2)}{\Delta_1-\Delta_2}, \end{aligned} \tag{39}$$

with the function F defined in Eq. (B4). The scale Δ in these functions results from the mass difference between the external and the internal heavy hadrons. In the heavy-quark and the isospin limits, we have

$$M_{B_d^*} - M_{B_u} = M_{S_{dd}} - M_{S_{du}} = 0.$$

Therefore, the only relevant heavy-hadron mass difference in these limits is

$$\Delta^{(B)} = M_{S_{du}} - M_{T_{du}} = M_{S_{dd}} - M_{T_{du}} \sim 200 \text{ MeV},$$

and the effective couplings in Eq. (38) are

$$\begin{aligned}
(g_1)_{\text{eff}} &= g_1\Big[1 - \frac{2}{f^2} I(M_\pi) + \frac{4g_1^2}{f^2} H(M_\pi, 0) \\
&\quad + \text{analytic terms}\Big], \\
(g_2)_{\text{eff}} &= g_2\Big[1 - \frac{2}{f^2} I(M_\pi) + \frac{3g_2^2}{2f^2} H(M_\pi, 0) \\
&\quad + \frac{g_3^2}{f^2}(H(M_\pi, -\Delta^{(B)}) - 2K(M_\pi, -\Delta^{(B)}, 0)) \\
&\quad + \text{analytic terms}\Big], \\
(g_3)_{\text{eff}} &= g_3\Big[1 - \frac{2}{f^2} I(M_\pi) + \frac{g_2^2}{f^2}(-2H(M_\pi, \Delta^{(B)}) \\
&\quad + H(M_\pi, 0)) + \frac{g_3^2}{2f^2}(H(M_\pi, -\Delta^{(B)}) \\
&\quad + 9H(M_\pi, \Delta(B)) - 2K(M_\pi, \Delta^{(B)}, 0)) \\
&\quad + \text{analytic terms}\Big],
\end{aligned} \tag{40}$$

with the analytic terms resulting from $\mathcal{N}^{(2)}$ in Eq. (38). Here, we stress that the tadpole diagram is the dominant one-loop contribution to the chiral expansion of $(g_1)_{\text{eff}}$. This is because the typical value of the coupling, $g_1^2 \sim 0.25$, is small, leading to the suppression of other diagrams in the above equation.[7] A numerical comparison of the individual contributions from different types of Feynman diagrams will be given in Sec. IV B.

Before proceeding with further discussion of the formulas in Eq. (40), we notice that the function $H(m, \Delta)$ can be related to $I(m)$ when $\Delta = 0$,

$$H(m, 0) = -I(m) = -\frac{m^2}{16\pi^2}\log\left(\frac{m^2}{\mu^2}\right). \tag{41}$$

This leads to the simplification of the chiral expansion of $(g_1)_{\text{eff}}$,

$$\begin{aligned}
(g_1)_{\text{eff}} &= g_1\Big[1 - \frac{2}{(4\pi f)^2} M_\pi^2 \log\left(\frac{M_\pi^2}{\mu^2}\right) \\
&\quad - \frac{4g_1^2}{(4\pi f)^2} M_\pi^2 \log\left(\frac{M_\pi^2}{\mu^2}\right) + c(\mu) M_\pi^2\Big].
\end{aligned} \tag{42}$$

The renormalization-scale dependence from the loop diagrams is cancelled by the coefficient, $c(\mu)$, of the analytic term which also encodes the contributions from the NLO Lagrangian.

In the following two subsections, we first address an issue related to the chiral limit of the formulas presented above, and then present an estimation for the numerical size of the one-loop corrections.

A. Wave-function renormalization and sunset diagrams in the chiral limit

As pointed out in Eqs. (39) and (40), the infinite-volume one-loop contributions from the wave-function renormalization and sunset diagrams can be written in terms of the functions H and K, which are obtained by taking derivatives of the function defined in Eq. (B4),

$$\begin{aligned}
F(m, \Delta) &= \frac{-1}{16\pi^2}\Big[\Big(m^2 - \frac{2\Delta^2}{3}\Big)\Delta \log\left(\frac{m^2}{\mu^2}\right) \\
&\quad + \Big(\frac{10\Delta^2}{9} - \frac{4m^2}{3}\Big)\Delta + \frac{2(\Delta^2 - m^2)}{3} m R\Big(\frac{\Delta}{m}\Big)\Big],
\end{aligned}$$

where $R(x) \equiv \sqrt{x^2 - 1}[\log(x - \sqrt{x^2 - 1 + i\epsilon}) - \log(x + \sqrt{x^2 - 1 + i\epsilon})]$.

This function is obtained by regularizing the loop integrals with the subtraction scheme defined in Eq. (B1) in Appendix B. Implementing this scheme is a common practice in χPT calculations [28]. It leads to the result that $F(m, \Delta)$ does not vanish in the limit $m \to 0$ unless $\Delta = 0$. Such behavior does not cause any conceptual problem in the effective theory, since the axial couplings, $g_{1,2,3}$, can undergo finite renormalization depending on the subtraction scheme used to regulate one-loop integrals. Various subtraction schemes always lead to the same physical quantities, such as the hadronic masses and axial transition amplitudes, which are scheme independent. On the other hand, it would be desirable and natural to choose a scheme in which the one-loop contributions decouple in the chiral limit. As pointed out in Refs. [29,30], it is possible to find a scheme such that the real part of F vanishes in the chiral limit. It is implemented by simply rewriting F as

$$\begin{aligned}
F^{(\text{sub})}(m, \Delta) &= \frac{-1}{16\pi^2}\Big[m^2\Delta \log\left(\frac{m^2}{\mu^2}\right) - \frac{2\Delta^3}{3}\log\left(\frac{m^2}{4\Delta^2}\right) \\
&\quad - \frac{4m^2\Delta}{3} + \frac{2(\Delta^2 - m^2)}{3} m R\Big(\frac{\Delta}{m}\Big)\Big],
\end{aligned} \tag{43}$$

and appropriately modifying the counterterms to absorb the difference (a finite polynomial in Δ). It is straightforward to demonstrate that when $\Delta + m > 0$, in which case the

[7] Since $g_{2,3} \sim O(1)$, this suppression is not present in the chiral expansion of $(g_{2,3})_{\text{eff}}$.

external heavy hadrons are stable particles, this function is real and

$$\lim_{m\to 0} F^{(\mathrm{sub})}(m, \Delta) = 0. \tag{44}$$

In the case $\Delta + m < 0$ which corresponds to the situation that the external heavy hadron becomes unstable, the functions F and $F^{(\mathrm{sub})}$ are complex. Although the real part of $F^{(\mathrm{sub})}$ vanishes in the chiral limit, the imaginary part remains nonzero. This occurs when

$$M_\pi < |M_{T_{ij}} - M_{S^\mu_{ij}}| = \Delta^{(B)} \sim 200 \text{ MeV}. \tag{45}$$

Below this threshold, one cannot define matrix elements containing external S^μ_{ij} hadrons. In principle, more complicated matrix elements can be used to determine the couplings g_2 and g_3 for the pion masses in the regime of Eq. (45), but this is beyond the scope of this work. See Refs. [31,32] for related discussions. Here, we stress that one can perform lattice calculations in the regime where the pion mass is larger than $\Delta^{(B)}$ but small compared to the chiral symmetry breaking scale, such that the external hadrons are all stable and the chiral expansion is still valid. These calculations enable the extraction of the axial couplings, $g_{1,2,3}$, which can then be used to perform chiral extrapolations and make predictions for other quantities.

B. Evaluation of individual contributions

In this subsection, we use the simple infinite volume, SU(2) case to explore the typical size of the one-loop contributions. This can be best summarized by the plots in Fig. 2. In these plots, the pion mass dependence of the loop contributions to three effective axial couplings [their real part in the case of $(g_{2,3})_{\mathrm{eff}}$] is shown for exemplary values of the various low-energy constants. These results are obtained using the subtraction scheme defined in Eq. (43) in Sec. IVA. The leading-order contribution is also shown. We take $g_1 = 0.5$, a value consistent with recent determinations [12–17], and then use the quark model expectations for the other couplings, $g_2 = 2g_1$ and $g_3 = \sqrt{2}g_1$ (in our normalization) [3][8] which are far less constrained. We work in the heavy-quark limit so that $\Delta^{(M)} = 0$, and we have set the $S - T$ mass differences to $\Delta^{(B)} = 200$ MeV, consistent with experiment [26]. The renormalization scale used here is $\mu = 4\pi f$.

It is clear from these figures that the tadpole contributions provide an important part of the chiral nonanalytic behavior of the axial couplings. Furthermore, in the range of pion masses considered here, $M_\pi \lesssim 400$ MeV, the NLO contributions from loops are numerically small corrections to the leading-order results.[9] This indicates that in this range the SU(2) chiral expansion of the axial-current matrix elements is well behaved. Variations of the low-energy constants, g_1, g_2, g_3, $\Delta^{(B)}$, and the renormalization scale, μ, within reasonable ranges do not substantially alter the behavior shown in Fig. 2.

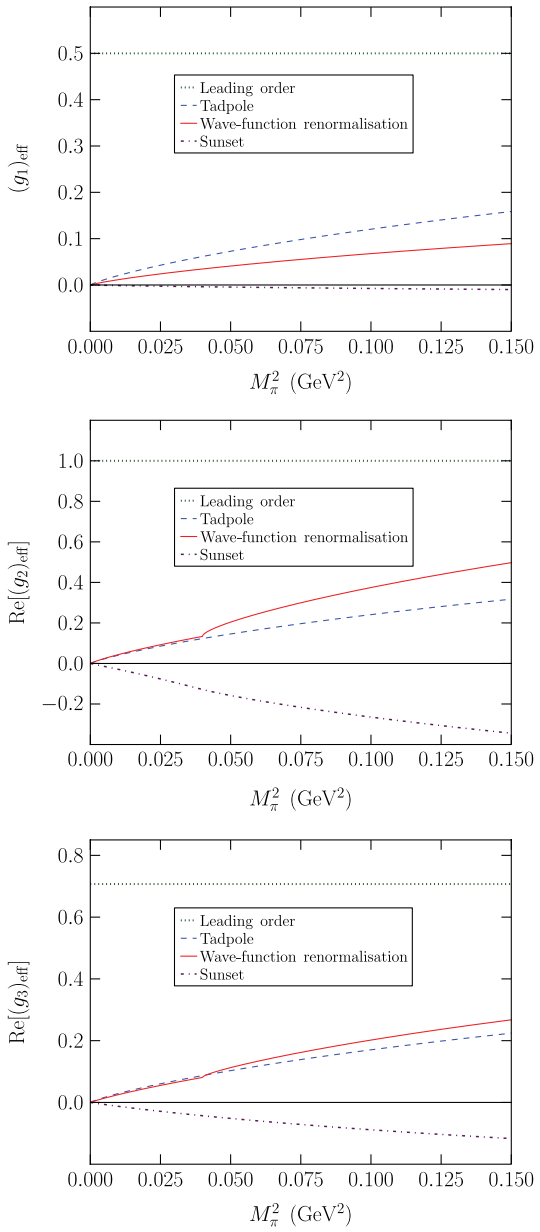

FIG. 2 (color online). Comparison of the individual infinite-volume one-loop contributions to the pion mass dependence of the (real part of the) various effective couplings, $(g_{1,2,3})_{\mathrm{eff}}$ evaluated using the values of the low-energy constants given in the text. The kinks in the wave-function renormalization and sunset contributions to the baryonic couplings arise from the $S \to T\pi$ threshold at $M_\pi = \Delta^{(B)}$. Below this threshold, the curves lose their physical interpretation. The subtraction scheme is that presented in Eq. (43).

[8]These values are also consistent with preliminary lattice QCD results [33].

[9]The imaginary parts of $(g_{2,3})_{\mathrm{eff}}$ that arise for $M_\pi < \Delta^{(B)}$ are also small, $|\mathrm{Im}(g_{2,3})_{\mathrm{eff}}| < 0.05$.

V. ONE-LOOP CONTRIBUTIONS IN SU(4|2) AND SU(6|3) HHχPT

In this section, we study the one-loop contributions in Eq. (32) in SU(4|2) and SU(6|3) partially quenched HHχPT in finite volume. These results are complicated because we keep the SU(3) light-flavor breaking effects from Eq. (26) in our calculation. Here, we investigate the structure of the one-loop computation via analyzing the quark-flavor flow picture [34]. The details of the results are given in Appendices C and D.

A. The tadpole diagrams

First, we present the contributions from the tadpole diagrams. These take the simple form,

$$\begin{aligned}
\mathcal{T}^{(2)}_{ud} &= -2J(M_{u,u'}), \qquad \mathcal{T}^{(3)}_{ud} = -2J(M_{u,u'}) - J(M_{u,s'}),\\
\mathcal{T}^{(3)}_{us} &= -J(M_{u,u'}) - \tfrac{1}{2}J(M_{u,s'}) - J(M_{s,u'}) - \tfrac{1}{2}J(M_{s,s'})\\
&\quad + \tfrac{1}{6}\tilde{J}_3(M_{u,u}) - \tfrac{1}{3}\tilde{J}_3(M_{u,s}) + \tfrac{1}{6}\tilde{J}_3(M_{s,s}),
\end{aligned} \tag{46}$$

where the functions J and $\tilde{J}_3$ are defined in (B3) and (B13), respectively. The tadpole-diagram results are completely determined by the structure of the axial currents.

B. The self-energy diagrams

In this subsection, we present the heavy-hadron wave-function renormalization, resulting from the self-energy diagrams. These are more complicated than the tadpole-diagram results in our calculation, since we keep track of the flavor SU(3) breaking effects from both the Goldstone masses [Eq. (3)] and the heavy-meson and baryon spectrum [Eq. (26)]. It is helpful to analyze the quark-flavor flow diagrams [34] to understand the structure of the results. To investigate this structure, we first assign a "direction" to each flavor flow line:

(i) The flow following the direction of a line means a quark with that flavor, while the flow against the direction means its antiquark.

For the analysis of the heavy-meson wave-function renormalization, we follow the nomenclature for the coefficients in front of the sum (integral) in a loop diagram:

(i) The "tilded" coefficients accompany the hairpin contributions from the light-flavor-singlet mesons.

(ii) The "primed" coefficients multiply the sums in which a B meson appears in the loop, while the "unprimed" coefficients are for the cases involving an internal B^* meson.

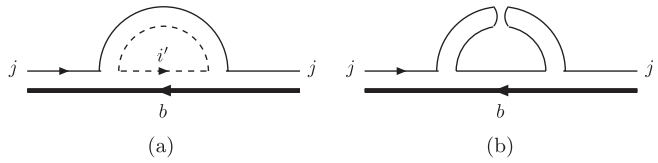

FIG. 3. Quark-flavor flow structure for the meson self-energy diagrams. The thick line represents the anti-b quark, and the thin lines are the valence light quarks, while the dashed line is the sea light quark. Diagram (a) contributes to the w and w' terms in Eq. (47) when the internal heavy-light meson is $B^*_{i'}$ and $B_{i'}$, respectively, while the Goldstone meson is composed of a j valence quark and an i' sea antiquark. Diagram (b) is the hairpin structure and results in terms containing $\tilde{w}$ (internal B^*_j) and $\tilde{w}'$ (internal B_j) in Eq. (47).

The quark flow picture for the heavy-meson wave-function renormalization diagrams is presented in Fig. 3. Since there is only one valence light quark involved, and the internal valence-quark loops are cancelled by the ghost-quark loops, the only possible nonhairpin structure is from the sea-quark contributions. This is depicted in Fig. 3(a), where the Goldstone meson is composed of a j valence quark, and an i' sea antiquark. The hairpin contribution is presented in Fig. 3(b).

Following the above nomenclature and the quark-flavor flow picture in Fig. 3, the results for the heavy-meson wave-function renormalization can be written as

$$\begin{aligned}
\mathcal{W}^{(N_f)}_{B_j} &= g_1^2 \sum_a [w^{(N_f)}_{B_j,a}\mathcal{H}(M_{j,a}, \Delta^{(M)} + \delta^{(M)}_{a,j})\\
&\quad + \tilde{w}^{(N_f)}_{B_j,a}\tilde{\mathcal{H}}_{N_f}(M_{j,a}, \Delta^{(M)})],\\
\mathcal{W}^{(N_f)}_{B^*_j} &= g_1^2 \sum_a [w^{\prime(N_f)}_{B^*_j,a}\mathcal{H}(M_{j,a}, -\Delta^{(M)} + \delta^{(M)}_{a,j})\\
&\quad + \tilde{w}^{\prime(N_f)}_{B^*_j,a}\tilde{\mathcal{H}}_{N_f}(M_{j,a}, -\Delta^{(M)}) + w^{(N_f)}_{B^*_j,a}\mathcal{H}(M_{j,a}, \delta^{(M)}_{a,j})\\
&\quad + \tilde{w}^{(N_f)}_{B^*_j,a}\tilde{\mathcal{H}}_{N_f}(M_{j,a}, 0)],
\end{aligned} \tag{47}$$

where the summations are over the flavors u and u' in the SU(4|2) theory, and are over the flavors u, s, u', and s' in the SU(6|3) theory. The functions $\mathcal{H}$ and $\tilde{\mathcal{H}}_{N_f}$ are results of the sums (integrals) involved in the loops, and are defined in Eqs. (B9) and (B11)–(B13) in Appendix B. The mass parameters $M_{j,a}$, $\Delta^{(M)}$, and $\delta^{(M)}_{a,j}$ are defined in Eq. (A1) in Appendix A. The coefficients w, w', $\tilde{w}$, and $\tilde{w}'$ are presented in Table I in Appendix C.

Next, we discuss the structure of the baryon self-energy diagrams. We start by modifying the above rule for assigning the primed coefficients,

TABLE I. Coefficients for heavy-light meson wave-function renormalization, in Eq. (47), in the isospin limit.

a	u	s	u'	s'
$w^{(2)}_{B_u,a}$	0	0	3	0
$\tilde{w}^{(2)}_{B_u,a}$	$\frac{-3}{4}$	0	0	0
$w^{(3)}_{B_u,a}$	0	0	3	$\frac{3}{2}$
$\tilde{w}^{(3)}_{B_u,a}$	$\frac{-1}{2}$	0	0	0
$w^{\prime(2)}_{B^*_d,a}$	0	0	1	0
$\tilde{w}^{\prime(2)}_{B^*_d,a}$	$\frac{-1}{4}$	0	0	0
$w^{(2)}_{B^*_d,a}$	0	0	2	0
$\tilde{w}^{(2)}_{B^*_d,a}$	$\frac{-1}{2}$	0	0	0
$w^{\prime(3)}_{B^*_d,a}$	0	0	1	$\frac{1}{2}$
$\tilde{w}^{\prime(3)}_{B^*_d,a}$	$\frac{-1}{6}$	0	0	0
$w^{(3)}_{B^*_d,a}$	0	0	2	1
$\tilde{w}^{(3)}_{B^*_d,a}$	$\frac{-1}{3}$	0	0	0
$w^{\prime(3)}_{B^*_s,a}$	0	0	1	$\frac{1}{2}$
$\tilde{w}^{\prime(3)}_{B^*_s,a}$	0	$\frac{-1}{6}$	0	0
$w^{(3)}_{B^*_s,a}$	0	0	2	1
$\tilde{w}^{(3)}_{B^*_s,a}$	0	$\frac{-1}{3}$	0	0

(i) The primed coefficients multiply the sums in which the T baryon appears in the loop, while the unprimed coefficients are for the cases involving the internal S baryon.

These diagrams are further complicated by the presence of two light valence quarks. To keep track of the flavor flow of these two quarks, we introduce an additional rule to our notation,

(i) For a baryon (T_{ij} or S_{ij}) of light-flavor indices i and j, we assign the coefficient u to the diagram if the quark carrying flavor i appears in the Goldstone meson. For all the other cases, including the appearance of the anti-i in the Goldstone meson, they are accompanied by the coefficient w.

The flavor flow structure for the baryon self-energy diagrams can be summarized in Figs. 4 and 5. For the diagrams explicitly shown in Figs. 4(a) and 4(b), the Goldstone mesons are composed of (j, anti-i) and (j, anti-i'), respectively. Therefore, they are accompanied by the w-type coefficients (w for the internal S baryon and w' for the internal T baryon). Terms with the u-type coefficients are obtained by exchanging the flavors i and j, as also indicated in this figure. Notice that the "nonhairpin" valence-valence Goldstone contributions appear via the "crossing" configuration in Fig. 4(a). The hairpin structure of the baryon self-energy diagrams is presented in Fig. 5. From the above rules, it is clear that the diagram in Fig. 5(a) leads to a $\tilde{w}$-type term, while those in Fig. 5(b) and 5(c) are multiplied by $\tilde{u}$-type coefficients.

Following the above discussion, we obtain the results for the baryon wave-function renormalization,

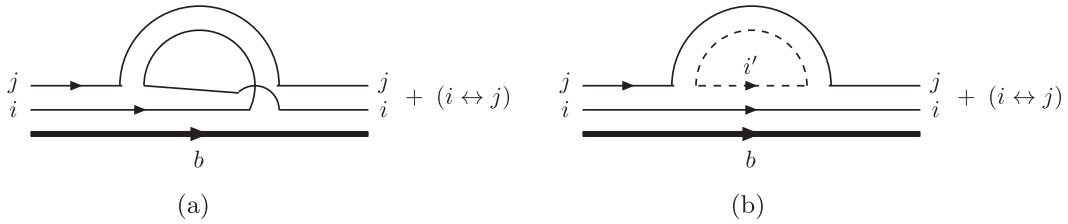

FIG. 4. Quark-flavor flow structure for the baryon self-energy diagrams without the hairpin structure. The thick line represents the b quark, and the thin lines are the valence light quarks, while the dashed line is the sea light quark. Diagram (a) is the crossing type which does not involve sea-quark contributions. The explicitly shown diagrams give rise to the terms multiplied by w and w' in Eq. (48) when the internal baryons are S_{ai} and T_{ai}, respectively [$a = i$ in diagram (a) and $a = i'$ in diagram (b)]. Interchanging the flavor indices i and j leads to the corresponding u and u' terms in the same equation.

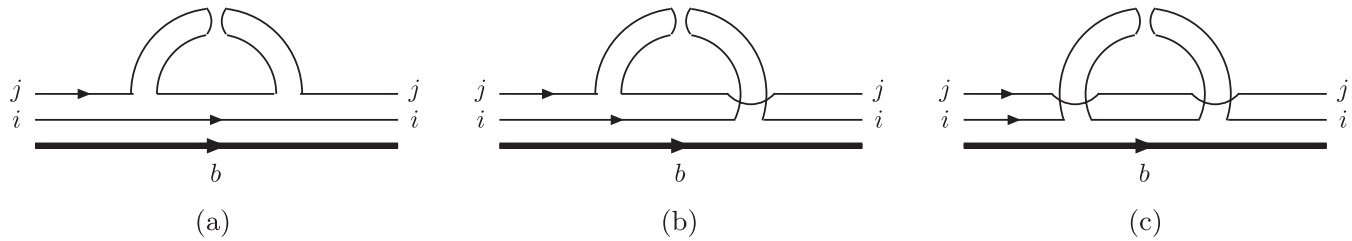

FIG. 5. Quark-flavor flow structure for the baryon self-energy diagrams involving the hairpin structure. The thick line represents the b quark, and the thin lines are the valence light quarks. Diagram (a) contributes to the $\tilde{w}$ (internal S_{ij} baryon) and $\tilde{w}'$ (internal T_{ij} baryon) terms in Eq. (48), while diagrams (b) and (c) result in the $\tilde{u}$ (internal S_{ij} baryon) and $\tilde{u}'$ (internal T_{ij} baryon) terms in the same equation.

TABLE II. Coefficients for T_{ij} baryon wave-function renormalization, in Eq. (48), in the isospin limit.

a	u	s	u'	s'
$w^{(2)}_{T_{du},a} + u^{(2)}_{T_{du},a}$	$\frac{3}{2}$	0	3	0
$\tilde{w}^{(2)}_{T_{du},a} + \tilde{u}^{(2)}_{T_{du},a}$	0	0	0	0
$w^{(3)}_{T_{du},a} + u^{(3)}_{T_{du},a}$	$\frac{3}{2}$	0	3	$\frac{3}{2}$
$\tilde{w}^{(3)}_{T_{du},a} + \tilde{u}^{(3)}_{T_{du},a}$	0	0	0	0
$w^{(3)}_{T_{su},a}$	0	$\frac{3}{4}$	$\frac{3}{2}$	$\frac{3}{4}$
$\tilde{w}^{(3)}_{T_{su},a}$	$\frac{-1}{4}$	0	0	0
$u^{(3)}_{T_{su},a}$	$\frac{3}{4}$	0	$\frac{3}{2}$	$\frac{3}{4}$
$\tilde{u}^{(3)}_{T_{su},a}$	$\frac{1}{2}$	$\frac{-1}{4}$	0	0

$$
\begin{aligned}
\mathcal{W}^{(N_f)}_{T_{ij}} &= g_3^2 \sum_a [w^{(N_f)}_{T_{ij},a} \mathcal{H}(M_{j,a}, \Delta^{(B)} + \delta^{(B)}_{ai,ij}) \\
&\quad + \tilde{w}^{(N_f)}_{T_{ij},a} \tilde{\mathcal{H}}_{N_f}(M_{j,a}, \Delta^{(B)}) \\
&\quad + u^{(N_f)}_{T_{ij},a} \mathcal{H}(M_{i,a}, \Delta^{(B)} + \delta^{(B)}_{aj,ij}) \\
&\quad + \tilde{u}^{(N_f)}_{T_{ij},a} \tilde{\mathcal{H}}_{N_f}(M_{i,a}, \Delta^{(B)})], \\
\mathcal{W}^{(N_f)}_{S_{ij}} &= g_2^2 \sum_a [w^{(N_f)}_{S_{ij},a} \mathcal{H}(M_{j,a}, \delta^{(B)}_{ai,ij}) + \tilde{w}^{(N_f)}_{S_{ij},a} \tilde{\mathcal{H}}_{N_f}(M_{j,a}, 0) \\
&\quad + u^{(N_f)}_{S_{ij},a} \mathcal{H}(M_{i,a}, \delta^{(B)}_{aj,ij}) + \tilde{u}^{(N_f)}_{S_{ij},a} \tilde{\mathcal{H}}_{N_f}(M_{i,a}, 0)] \\
&\quad + g_3^2 \sum_a [w^{\prime(N_f)}_{S_{ij},a} \mathcal{H}(M_{j,a}, -\Delta^{(B)} + \delta^{(B)}_{ai,ij}) \\
&\quad + \tilde{w}^{\prime(N_f)}_{S_{ij},a} \tilde{\mathcal{H}}_{N_f}(M_{j,a}, -\Delta^{(B)}) \\
&\quad + u^{\prime(N_f)}_{S_{ij},a} \mathcal{H}(M_{i,a}, -\Delta^{(B)} + \delta^{(B)}_{aj,ij}) \\
&\quad + \tilde{u}^{\prime(N_f)}_{S_{ij},a} \tilde{\mathcal{H}}_{N_f}(M_{i,a}, -\Delta^{(B)})], \qquad (48)
\end{aligned}
$$

where the summations are over the flavors u and u' in the SU(4|2) theory, and are over the flavors u, s, u', and s' in the SU(6|3) theory. The relevant coefficients, w, $u \ldots$ are presented in Tables II and III in Appendix C. The mass parameters $M_{a,b}$, $\Delta^{(B)}$, and $\delta^{(B)}_{ab,cd}$ are defined in Eq. (A1) in Appendix A. These results agree with those in the literature [35].[10]

C. The sunset diagrams

In this subsection, we discuss the structure of the sunset diagrams. The Lorentz indices carried by the hadronic states are completely absorbed into the tree-level contribution in Eq. (32), therefore they are omitted in the notation below. In order to organize the results, we follow the same convention in assigning the "flow direction" to a quark line and the tilded coefficients to the terms involving the hairpin structure, as that in the self-energy diagrams.

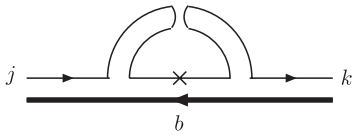

FIG. 6. Quark-flavor flow structure for the meson sunset diagrams with external B_j and B^*_k states. The thick line represents the anti-b quark, and the thin line is the valence light quark. The cross is the current J_{jk}. This diagram results in the $\tilde{y}$ (internal B^*_j and B^*_k) and $\tilde{y}'$ (internal B^*_j and B_k) terms in Eq. (49). This is the only possible quark-flavor flow configuration for the meson sunset diagrams.

First, we study the sunset diagram for the axial-current matrix element between the B_j and B^*_k mesons. Because of the flavor-changing structure of the currents that we consider in this work, it is straightforward to demonstrate that in this case the Goldstone meson must involve the hairpin contribution. This is depicted in Fig. 6. Furthermore, the internal heavy meson with the light flavor j must be a B^*_j since there is no $B - B$Goldstone coupling in the Lagrangian or the current. On the other hand, the internal heavy meson involving the light flavor k can be either B_k or B^*_k. These two cases are distinguished by the primed and the unprimed coefficients in the results. We then obtain the sunset-diagram contribution to this matrix element as

$$
\begin{aligned}
\mathcal{Q}^{(N_f)}_{B_j \to B^*_k} &= g_1^2 [\tilde{y}^{(N_f)}_{B_j,B^*_k} \tilde{\mathcal{K}}_{N_f}(M_{j,k}, \Delta^{(M)}, \Delta^{(M)} + \delta^{(M)}_{k,j}) \\
&\quad + \tilde{y}^{\prime(N_f)}_{B_j,B^*_k} \tilde{\mathcal{K}}_{N_f}(M_{j,k}, \Delta^{(M)}, \delta^{(M)}_{k,j})], \qquad (49)
\end{aligned}
$$

where $\mathcal{K}$ and $\tilde{\mathcal{K}}_{N_f}$ are the sums (integrals) involved in the loops, and are defined in Eqs. (B9) and (B11)–(B13) in Appendix B. The mass parameters $M_{j,k}$, $\Delta^{(M)}$, and $\delta^{(M)}_{k,j}$ are defined in Eq. (A1) in Appendix A. The coefficients $\tilde{y}$ and $\tilde{y}'$ are presented in Table VII in Appendix D.

Next, we investigate the sunset diagrams for the following axial-current transitions involving baryons,

$$
T_{ij} \to S^\mu_{ik} \qquad S^\mu_{ij} \to S^\nu_{ik}, \qquad (50)
$$

where the spectator quark carries the flavor index i. The quark-flavor flow configurations are shown in Figs. 7–9. Again, we use the tilded coefficients to denote terms in which the hairpin structure appears. Because of parity,

[10]The SU(3) breaking effects arising from Eq. (26) are not included in the results in Ref. [35]. We have also checked these wave-function renormalization diagrams against the full-QCD, SU(3)-limit results at $\Delta^{(B)} = 0$ in Ref. [5], and found agreement.

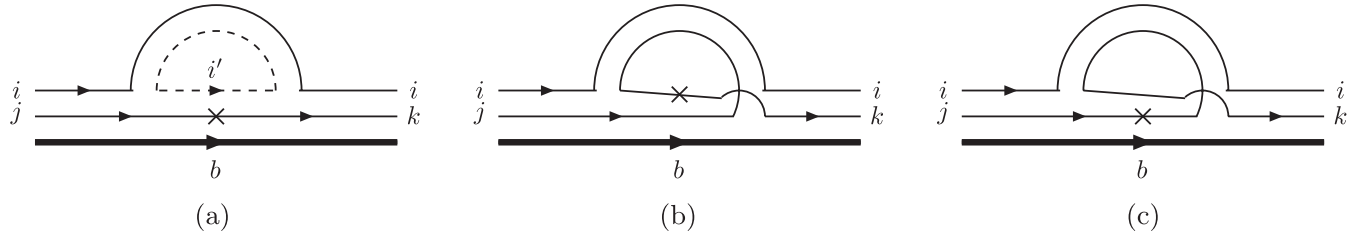

FIG. 7. Quark-flavor flow structure for the baryon sunset diagrams without the hairpin structure. The thick line represents the b quark, and the thin lines are the valence light quarks, while the dashed line is the sea light quark. The cross is the current J_{jk}. These diagrams lead to the x [internal S_{aj} and S_{ak} baryons with $a = i', j, k$ in diagrams (a), (b), (c), respectively], x' (internal T_{aj} and S_{ak} baryon), and x'' (internal S_{aj} and T_{ak} baryons) terms in Eq. (51).

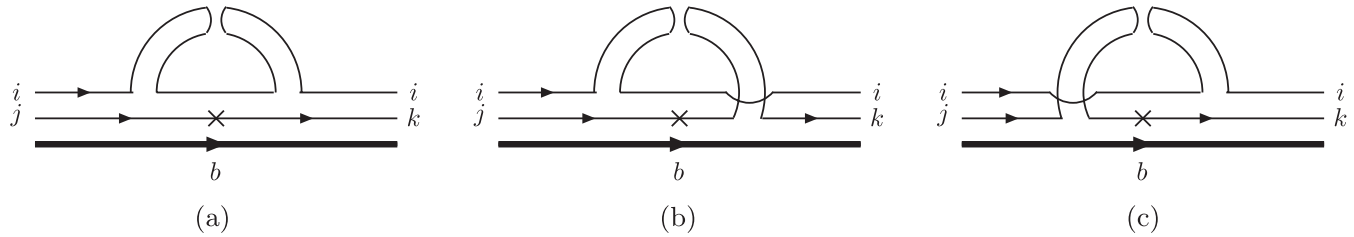

FIG. 8. Quark-flavor flow structure for the baryon sunset diagrams with the hairpin structure involving the spectator quark (flavor i). The thick line represents the b quark, and the thin lines are the valence light quarks. The cross is the current J_{jk}. These diagrams lead to the $\tilde{x}$ (internal S_{ij} and S_{ik} baryons), $\tilde{x}'$ (internal T_{ij} and S_{ik} baryon), and $\tilde{x}''$ (internal S_{ij} and T_{ik} baryons) terms in Eq. (51).

there are no axial couplings amongst even numbers of Goldstone mesons, therefore the flavor indices j and k must appear in the internal baryons. These internal baryons can be T or S type. Denoting the other flavor index in the loop by a, we adopt the following convention to distinguish various possibilities for the internal S and T contributions:

(i) If the internal baryons are S_{aj} and S_{ak}, then the coefficient for the diagram is unprimed.

(ii) If the internal baryons are T_{aj} (left in the loop) and S_{ak} (right in the loop), then the coefficient for the diagram is primed. Such terms are absent in the $T \to S$ transition amplitudes.

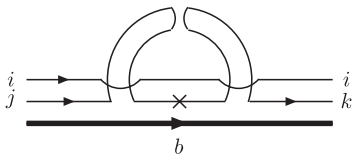

FIG. 9. Quark-flavor flow structure for the baryon sunset diagrams with the hairpin structure in which the spectator quark (flavor i) is absent. The thick line represents the b quark, and the thin lines are the valence light quarks. The cross is the current J_{jk}. These diagrams lead to the $\tilde{y}$ (internal S_{ij} and S_{ik} baryons), $\tilde{y}'$ (internal T_{ij} and S_{ik} baryon), and $\tilde{y}''$ (internal S_{ij} and T_{ik} baryons) terms in Eq. (51).

(iii) If the internal baryons are S_{aj} (left in the loop) and T_{ak} (right in the loop), then the coefficient for the diagram is "double-primed."

To keep track of the flow of the spectator quark i in these processes, we follow the rules:

(i) If the spectator quark flavor is present in the Goldstone meson, then the diagram corresponds to a term with x-type coefficient (x, x', x'', $\tilde{x}$, $\tilde{x}'$, or $\tilde{x}''$).

(ii) If the spectator quark flavor is absent in the Goldstone meson, then the diagram corresponds to a term with y-type coefficient.

In Fig. 7, we show the quark-flavor flow diagrams containing no hairpin structure. In such flow configurations, the spectator quark flavor always appears in the Goldstone meson. Therefore, they will only be accompanied by the x-type coefficients. Notice that the valence-valence Goldstone mesons also appear in these diagrams via the crossing configurations in Figs. 7(b) and 7(c). The hairpin contributions to the quark-flavor flow configurations for the processes in Eq. (50) are shown in Figs. 8 and 9. These two figures are distinguished by the presence/absence of the spectator quark flavour in the Goldstone propagator. Therefore, they correspond to terms with $\tilde{x}$- and $\tilde{y}$-type coefficients, respectively.

Following the above rules in analyzing the quark-flavor flow structure, the results for the baryon sunset diagrams can be written as

$$\mathcal{Q}^{(N_f)}_{T_{ij}\to S_{ik}} = g_2^2\Big\{\sum_a [x^{(N_f)}_{T_{ij},S_{ik},a}\mathcal{K}(M_{i,a},\Delta^{(B)}+\delta^{(B)}_{aj,ij},\Delta^{(B)}+\delta^{(B)}_{ak,ij}) + \tilde{x}^{(N_f)}_{T_{ij},S_{ik},a}\tilde{\mathcal{K}}_{N_f}(M_{i,a},\Delta^{(B)},\Delta^{(B)}+\delta^{(B)}_{ik,ij})]$$
$$+ \tilde{y}^{(N_f)}_{T_{ij},S_{ik}}\tilde{\mathcal{K}}_{N_f}(M_{j,k},\Delta^{(B)},\Delta^{(B)}+\delta^{(B)}_{ik,ij})\Big\} + g_3^2\Big\{\sum_a [x^{\prime\prime(N_f)}_{T_{ij},S_{ik},a}\mathcal{K}(M_{i,a},\Delta^{(B)}+\delta^{(B)}_{aj,ij},\delta^{(B)}_{ak,ij})$$
$$+ \tilde{x}^{\prime\prime(N_f)}_{T_{ij},S_{ik},a}\tilde{\mathcal{K}}_{N_f}(M_{i,a},\Delta^{(B)},\delta^{(B)}_{ik,ij})] + \tilde{y}^{\prime\prime(N_f)}_{T_{ij},S_{ik}}\tilde{\mathcal{K}}_{N_f}(M_{j,k},\Delta^{(B)},\delta^{(B)}_{ik,ij})\Big\},$$
$$\mathcal{Q}^{(N_f)}_{S_{ij}\to S_{ik}} = g_2^2\Big\{\sum_a [x^{(N_f)}_{S_{ij},S_{ik},a}\mathcal{K}(M_{i,a},\delta^{(B)}_{aj,ij},\delta^{(B)}_{ak,ij}) + \tilde{x}^{(N_f)}_{S_{ij},S_{ik},a}\tilde{\mathcal{K}}_{N_f}(M_{i,a},0,\delta^{(B)}_{ik,ij})] + \tilde{y}^{(N_f)}_{S_{ij},S_{ik}}\tilde{\mathcal{K}}_{N_f}(M_{j,k},0,\delta^{(B)}_{ik,ij})\Big\}$$
$$+ g_3^2\Big\{\sum_a [x^{\prime(N_f)}_{S_{ij},S_{ik},a}\mathcal{K}(M_{i,a},-\Delta^{(B)}+\delta^{(B)}_{aj,ij},\delta^{(B)}_{ak,ij}) + \tilde{x}^{\prime(N_f)}_{S_{ij},S_{ik},a}\tilde{\mathcal{K}}_{N_f}(M_{i,a},-\Delta^{(B)},\delta^{(B)}_{ik,ij})] + \tilde{y}^{\prime(N_f)}_{S_{ij},S_{ik}}\tilde{\mathcal{K}}_{N_f}(M_{j,k},-\Delta^{(B)},\delta^{(B)}_{ik,ij})$$
$$\times\sum_a [x^{\prime\prime(N_f)}_{S_{ij},S_{ik},a}\mathcal{K}(M_{i,a},\delta^{(B)}_{aj,ij},-\Delta^{(B)}+\delta^{(B)}_{ak,ij}) + \tilde{x}^{\prime\prime(N_f)}_{S_{ij},S_{ik},a}\tilde{\mathcal{K}}_{N_f}(M_{i,a},0,-\Delta^{(B)}+\delta^{(B)}_{ik,ij})]$$
$$+ \tilde{y}^{\prime\prime(N_f)}_{S_{ij},S_{ik}}\tilde{\mathcal{K}}_{N_f}(M_{j,k},0,-\Delta^{(B)}+\delta^{(B)}_{ik,ij})\Big\}, \tag{51}$$

where the summations are over the flavors u and u' in the SU(4|2) theory, and are over the flavors u, s, u', and s' in the SU(6|3) theory. The relevant coefficients are presented in Tables IV, V, VI, VII, VIII, IX, and X in Appendix D.

VI. $H_1 \to H_2\pi(K)$ TRANSITION AMPLITUDES

The axial-current matrix elements, presented in the previous sections, are closely related to those in the strong-decay amplitudes, such as

$$B_d^* \to B_u\pi, \quad B_s^* \to B_u K, \quad \Sigma_b^{(*)} \to \Lambda_b\pi, \quad \Sigma_b^* \to \Sigma_b\pi. \tag{52}$$

Note that, with the exception of $\Sigma_b^{(*)} \to \Lambda_b\pi$, for bottom hadrons the above decays are kinematically forbidden in nature. In HHχPT, the LO and NLO analytic terms for these decay amplitudes have the same structure as the matrix elements in Eq. (32). That is, the LO contributions are all proportional to the axial couplings $g_{1,2,3}$, while the NLO results are polynomials in the Goldstone masses. Therefore, we only address the one-loop diagrams for these decays.

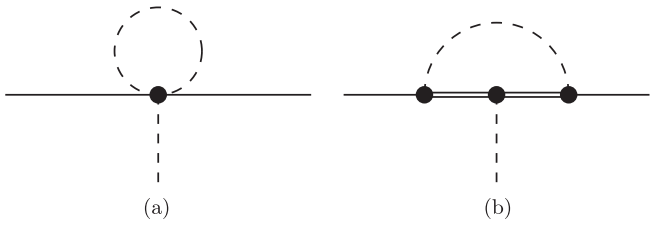

FIG. 10. Diagrams contributing to the decay amplitudes in Eq. (52). The self-energy diagrams leading to wave-function renormalization of the external particles are not shown in this figure. The dashed lines are the Goldstone mesons. The single solid lines denote generically the external heavy hadrons, while the double solid lines are the internal heavy hadrons. They can be B, B^* mesons or T_{ij}, S_{ij} baryons. The vertices are all from the axial-coupling terms proportional to $g_{1,2,3}$ in the strong chiral Lagrangian in Eq. (24). Diagrams (a) and (b) are the tadpole and sunset types, respectively.

To compute the one-loop amplitudes for the processes in Eq. (52), one has to calculate the wave-function renormalization of the Goldstone bosons and the heavy hadrons, as well as the tadpole and sunset diagrams in Fig. 10. The Goldstone boson wave-function renormalization can be found in standard references such as [6,20], and the heavy-hadron wave-function renormalization is presented in Eqs. (47) and (48). The amplitudes from the sunset diagram in Fig. 10(b) are identical to those from the corresponding diagram in Fig. 1(c). Therefore, they are equal to the results presented in Eqs. (49) and (51). The tadpole diagram in Fig. 10(a) differs from that of the axial-current matrix elements in Fig. 1(b) by a factor of $1/3$. That is, one can take the results in Eq. (46), and multiply them by $1/3$ to obtain the corresponding tadpole-diagram contributions to the decay amplitudes in Eq. (52). It turns out that the contribution from the tadpole diagram is exactly cancelled by the contribution from the wave-function renormalization of the external Goldstone boson [36]. As is shown in Fig. 2, the tadpole diagrams provide significant contributions to the axial-current matrix elements and will lead to significant differences between the quark-mass dependence of axial-current matrix elements and that of strong-decay amplitudes.

These decay amplitudes have also been computed in Ref. [36], to one-loop order in SU(3) HHχPT in the infinite-volume limit with $\Delta^{(M)} = \Delta^{(B)} = 0$, and without the SU(3) breaking effects from the Lagrangian in Eq. (26). Our results agree with those presented in Ref. [36] in the same limits.

VII. CONCLUSION

With the expectation of precise data from the LHCb collaboration and from the potential SuperB experiment, accurate QCD calculations of quantities involving B mesons and single-b baryons will be important in further constraining flavor physics and in looking for physics beyond the SM. This is a challenging but necessary task. In this paper, we have presented calculations for axial-current matrix elements involving single heavy-hadron external states in HHχPT at the NLO. We have performed these computations in partially quenched χPT for both $N_f = 2$ and $N_f = 2 + 1$, including finite-volume effects. Our results are essential for extracting the axial couplings in HHχPT from experimental data or lattice QCD. These axial couplings are central quantities in b physics, as they control the light-quark-mass dependence of b-hadron observables and determine the strong-decay widths of heavy hadrons.

We have discussed the SU(2) case in detail, numerically analyzing the behavior of the various loop contributions for natural values of the low-energy constants. Based on our study, we conclude that the SU(2) chiral expansion of the axial-current matrix elements is well behaved for $M_\pi \lesssim 400$ MeV. This implies that lattice calculations that are performed in this regime can be used to determine the axial couplings reliably.

ACKNOWLEDGMENTS

We warmly thank Brian Tiburzi, André Walker-Loud, and Matthew Wingate for helpful discussions. This work is supported by U.S. DOE Contract No. DE-AC05-06OR-23177, Grants No. DE-SC000-1784 and No. DE-FG02-04ER41302, Jeffress Memorial Trust Grant No. J-968, and Taiwanese NSC Grant No. 99-2112-M-009-004-MY3. We acknowledge the hospitality of Academia Sinica Taipei, The College of William and Mary, Thomas Jefferson National Accelerator Facility, National Center of Theoretical Sciences, and National Chiao-Tung University.

APPENDIX A: MASS PARAMETERS

In this appendix, we define various quantities appearing in our results. First, we present the hadron masses,

$$\begin{aligned}
&M_{a,b}^2 = B_0(m_a + m_b), \quad \tilde{\delta}_{VS}^2 = M_{u,u}^2 - M_{u,u'}^2, \\
&\tilde{\delta}_{VSs}^2 = M_{s,s}^2 - M_{s,s'}^2, \quad M_X^2 = \tfrac{1}{3}(M_{u,u}^2 + 2M_{s,s}^2 - 2\tilde{\delta}_{VS}^2 - 4\tilde{\delta}_{VSs}^2), \\
&\Delta^{(M)} = M_{B_a^*} - M_{B_b}, \quad \delta_{a,b}^{(M)} = M_{B_a} - M_{B_b} = M_{B_a^*} - M_{B_b^*}, \\
&\Delta^{(B)} = M_{S_{ab}} - M_{T_{ab}}, \quad \delta_{ab,cd}^{(B)} = M_{T_{ab}} - M_{T_{cd}} = M_{S_{ab}} - M_{S_{cd}},
\end{aligned} \tag{A1}$$

where B_0 is defined in Eq. (6). As explained in the main text, $\Delta^{(M)}$ vanishes in the heavy-quark limit, while $\Delta^{(B)}$ remains nonzero and is of $O(\Lambda_{\rm QCD})$. In this paper, we work in the isospin limit, and denote the pion mass as $M_{u,u}$.

It is useful to define the following quantities which appear in the hairpin contributions to the flavor-singlet meson propagators in the SU(6|3) theory.

$$\begin{aligned}
A_{u,u} &= \frac{2(\tilde{\delta}_{VS}^2 - M_{u,u}^2 + M_X^2)\tilde{\delta}_{VS}^2}{(M_{u,u}^2 - M_X^2)^2} + \frac{3}{2}, \\
A_{s,s} &= \frac{3(8\tilde{\delta}_{VSs}^4 + (2\tilde{\delta}_{VS}^2 - M_{u,u}^2 + M_{s,s}^2)^2)}{(2\tilde{\delta}_{VS}^2 + 4\tilde{\delta}_{VSs}^2 - M_{u,u}^2 + M_{s,s}^2)^2}, \\
C_{u,u} &= 3\tilde{\delta}_{VS}^2 - \frac{2\tilde{\delta}_{VS}^4}{M_{u,u}^2 - M_X^2}, \\
C_{s,s} &= \frac{6\tilde{\delta}_{VSs}^2(2\tilde{\delta}_{VS}^2 - M_{u,u}^2 + M_{s,s}^2)}{2\tilde{\delta}_{VS}^2 + 4\tilde{\delta}_{VSs}^2 - M_{u,u}^2 + M_{s,s}^2}, \\
D_{u,s}^{(u)} &= \frac{2\tilde{\delta}_{VS}^2(M_{u,u}^2 - M_{s,s}^2 + 2\tilde{\delta}_{VSs}^2)}{(M_{u,u}^2 - M_{s,s}^2)(M_{u,u}^2 - M_X^2)}, \\
D_{u,s}^{(s)} &= \frac{2\tilde{\delta}_{VSs}^2(M_{u,u}^2 - M_{s,s}^2 - 2\tilde{\delta}_{VS}^2)}{(M_{u,u}^2 - M_{s,s}^2)(M_{s,s}^2 - M_X^2)}, \\
D_{u,s}^{(X)} &= \frac{(M_{u,u}^2 - M_X^2 - 2\tilde{\delta}_{VS}^2)(M_{s,s}^2 - M_X^2 - 2\tilde{\delta}_{VSs}^2)}{(M_{u,u}^2 - M_X^2)(M_{s,s}^2 - M_X^2)}.
\end{aligned} \tag{A2}$$

In the full-QCD limit, where $m_{u'} = m_u$ and $m_{s'} = m_s$,

$$\begin{aligned}
&A_{u,u}^{\rm QCD} = \tfrac{3}{2}, \quad A_{s,s}^{\rm QCD} = 3, \quad C_{u,u}^{\rm QCD} = 0, \quad C_{s,s}^{\rm QCD} = 0, \\
&D_{u,s}^{(u)\rm QCD} = 0, \quad D_{u,s}^{(s)\rm QCD} = 0, \quad D_{u,s}^{(X)\rm QCD} = 1.
\end{aligned} \tag{A3}$$

APPENDIX B: INTEGRALS AND SUMS

In this appendix, we present results of loop integrals and sums using dimensional regularization, with the ultraviolet divergences removed by subtracting the term,

$$\bar{\lambda} = \frac{2}{4-d} - \gamma_E + \log(4\pi) + 1, \tag{B1}$$

where d is the number of space-time dimensions. This is a commonly used scheme in χPT calculations [28]. It is different from the $\overline{\rm MS}$ scheme by the constant "1" on the right-hand side of the above equation. It can also be changed into the scheme discussed in Sec. IV A straightforwardly. Finite-volume effects in the limit $mL \gg 1$ (m is a generic Goldstone mass and L is the spatial lattice volume) are computed by replacing the momentum integrals by sums in the spatial directions. The one-loop contributions appearing in this work can all be obtained by investigating the following sums/integrals,

$$\mathcal{I}(m) \equiv \mu^{4-d} \oint\!\!\!\!\!\!\int \frac{d^d k}{(2\pi)^d} \frac{i}{k^2 - m^2 + i\epsilon} - \frac{m^2}{16\pi^2}\bar{\lambda},$$
$$\mathcal{F}(m,\Delta) \equiv (g^{\rho\nu} - v^\rho v^\nu)\left[\frac{\mu^{4-d}}{(d-1)} \oint\!\!\!\!\!\!\int \frac{d^d k}{(2\pi)^d} \frac{ik_\rho k_\nu}{(k^2 - m^2 + i\epsilon)(v\cdot k - \Delta + i\epsilon)} + \frac{g_{\rho\nu}}{16\pi^2}\bar{\lambda}\left(\frac{2\Delta^2}{3} - m^2\right)\Delta\right], \tag{B2}$$

where μ is the renormalization scale, and the symbol

$$\oint\!\!\!\!\!\!\int d^d k$$

means performing the sums in three spatial directions using the Poisson summation formula, followed by dimensionally regularizing the infinite-volume integrals.

We can further separate the infinite-volume limit of $\mathcal{I}$ and $\mathcal{F}$ from the finite-volume contributions,

$$\mathcal{I}(m) = I(m) + I_{\rm FV}(m), \qquad \mathcal{F}(m) = F(m,\Delta) + F_{\rm FV}(m). \tag{B3}$$

The functions I and F are results from the ordinary one-loop integrals,

$$I(m) = \frac{m^2}{16\pi^2}\log\left(\frac{m^2}{\mu^2}\right), \quad F(m,\Delta) = \frac{-1}{16\pi^2}\left[\left(m^2 - \frac{2\Delta^2}{3}\right)\Delta\log\left(\frac{m^2}{\mu^2}\right) + \left(\frac{10\Delta^2}{9} - \frac{4m^2}{3}\right)\Delta + \frac{2(\Delta^2 - m^2)}{3} mR\left(\frac{\Delta}{m}\right)\right], \tag{B4}$$

with

$$R(x) \equiv \sqrt{x^2-1}[\log(x - \sqrt{x^2 - 1 + i\epsilon}) - \log(x + \sqrt{x^2 - 1 + i\epsilon})]. \tag{B5}$$

The function $F(m,\Delta)$ does not vanish in the $m \to 0$ limit unless $\Delta = 0$. One can adopt the scheme discussed in Sec. IV A by simply rewriting F as $F^{(\rm sub)}$ defined in Eq. (43), and the real part of the function $F^{(\rm sub)}$ is zero in the chiral limit for arbitrary Δ.

For the case in which the external hadrons are stable particles, the finite-volume pieces can be shown to be [9,37][11]

$$I_{\rm FV}(m) = \frac{m}{4\pi^2}\sum_{\vec{u}\neq\vec{0}} \frac{1}{uL} K_1(umL) \overset{mL\gg 1}{\to} \frac{1}{4\pi^2}\sum_{\vec{u}\neq\vec{0}} \sqrt{\frac{m\pi}{2uL}}\left(\frac{1}{uL}\right) e^{-umL} \times \left\{1 + \frac{3}{8umL} - \frac{15}{128(umL)^2} + \mathcal{O}\left(\left[\frac{1}{umL}\right]^3\right)\right\},$$
$$F_{\rm FV}(m,\Delta) = \frac{-1}{12\pi^2}\sum_{\vec{u}\neq\vec{0}} \frac{1}{uL}\int_0^\infty d|\vec{k}| \frac{|\vec{k}|\sin(u|\vec{k}|L)}{\sqrt{|\vec{k}|^2 + m^2} + \Delta}\left(\Delta + \frac{m^2}{\sqrt{|\vec{k}|^2 + m^2}}\right) \overset{mL\gg 1}{\to} \frac{-m^2}{24\pi}\sum_{\vec{u}\neq\vec{0}} \frac{e^{-umL}}{uL}\mathcal{A}, \tag{B6}$$

where $\vec{u} = (u_1, u_2, u_3)$ with $u_i \in \mathbb{Z}$, $u \equiv |\vec{u}|$ and

$$\mathcal{A} = e^{(z^2)}[1 - \mathrm{Erf}(z)] + \left(\frac{1}{umL}\right)\left[\frac{1}{\sqrt{\pi}}\left(\frac{9z}{4} - \frac{z^3}{2}\right) + \left(\frac{z^4}{2} - 2z^2\right)e^{(z^2)}[1 - \mathrm{Erf}(z)]\right]$$
$$- \left(\frac{1}{umL}\right)^2\left[\frac{1}{\sqrt{\pi}}\left(-\frac{39z}{64} + \frac{11z^3}{32} - \frac{9z^5}{16} + \frac{z^7}{8}\right) - \left(-\frac{z^6}{2} + \frac{z^8}{8}\right)e^{(z^2)}[1 - \mathrm{Erf}(z)]\right] + \mathcal{O}\left(\frac{1}{(umL)^3}\right), \tag{B7}$$

with

[11] Similar formulas for finite-volume effects are also obtained in Ref. [38].

$$z = \left(\frac{\Delta}{m}\right)\sqrt{\frac{umL}{2}}. \tag{B8}$$

Higher-order terms in the $1/(umL)$ expansion in Eq. (B7) can be easily calculated. The integer u_i can be interpreted as the number of times that the pion wraps around the spatial volume in the i direction.

The functions appearing in our one-loop results are

$$\begin{aligned}
\mathcal{H}(m,\Delta) &\equiv \frac{\partial \mathcal{F}(m,\Delta)}{\partial \Delta} \quad \text{and} \\
\mathcal{K}(m,\Delta_1,\Delta_2) &\equiv \frac{\mathcal{F}(m,\Delta_1)-\mathcal{F}(m,\Delta_2)}{\Delta_1-\Delta_2}, \\
\mathcal{I}_{\eta'}(m) &\equiv \frac{\partial \mathcal{I}(m)}{\partial m^2}, \\
\mathcal{H}_{\eta'}(m,\Delta) &\equiv \frac{\partial \mathcal{H}(m,\Delta)}{\partial m^2}, \quad \text{and} \\
\mathcal{K}_{\eta'}(m,\Delta_1,\Delta_2) &\equiv \frac{\partial \mathcal{K}(m,\Delta_1,\Delta_2)}{\partial m^2}.
\end{aligned} \tag{B9}$$

Notice that

$$\mathcal{K}(m,\Delta,\Delta) \equiv \lim_{\Delta'\to\Delta} \mathcal{K}(m,\Delta,\Delta') = \mathcal{H}(m,\Delta). \tag{B10}$$

To present the residual flavor-singlet hairpin contributions in a compact form, we define three functions,

$$\tilde{\mathcal{I}}_{N_f}(m), \qquad \tilde{\mathcal{H}}_{N_f}(m,\Delta), \quad \text{and} \quad \tilde{\mathcal{K}}_{N_f}(m,\Delta_1,\Delta_2). \tag{B11}$$

They take the explicit form

$$\begin{aligned}
\tilde{\mathcal{I}}_2(m) &= \mathcal{I}(m) + 2\tilde{\delta}^2_{VS}\mathcal{I}_{\eta'}(m), \\
\tilde{\mathcal{H}}_2(m,\Delta) &= \mathcal{H}(m,\Delta) + 2\tilde{\delta}^2_{VS}\mathcal{H}_{\eta'}(m,\Delta), \\
\tilde{\mathcal{K}}_2(m,\Delta_1,\Delta_2) &= \mathcal{K}(m,\Delta_1,\Delta_2) + 2\tilde{\delta}^2_{VS}\mathcal{K}_{\eta'}(m,\Delta_1,\Delta_2),
\end{aligned} \tag{B12}$$

in the SU(4|2) theory ($N_f = 2$) where the mass m in the arguments is always equal to $M_{u,u}$, and

$$\begin{aligned}
\tilde{\mathcal{I}}_3(M_{a,b}) &= \delta_{a,b}\{A_{a,b}\mathcal{I}(M_{a,b}) + (1-A_{a,b})\mathcal{I}(M_X) \\
&\quad + C_{a,b}\mathcal{I}_{\eta'}(M_{a,b})\} \\
&\quad + (1-\delta_{a,b})\{D^{(a)}_{a,b}\mathcal{I}(M_{a,a}) \\
&\quad + D^{(b)}_{a,b}\mathcal{I}(M_{b,b}) + D^{(X)}_{a,b}\mathcal{I}(M_X)\}, \\
\tilde{\mathcal{H}}_3(M_{a,b},\Delta) &= \delta_{a,b}\{A_{a,b}\mathcal{H}(M_{a,b},\Delta) \\
&\quad + (1-A_{a,b})\mathcal{H}(M_X,\Delta) \\
&\quad + C_{a,b}\mathcal{H}_{\eta'}(M_{a,b},\Delta)\} \\
&\quad + (1-\delta_{a,b})\{D^{(a)}_{a,b}\mathcal{H}(M_{a,a},\Delta) \\
&\quad + D^{(b)}_{a,b}\mathcal{H}(M_{b,b},\Delta) + D^{(X)}_{a,b}\mathcal{H}(M_X,\Delta)\}, \\
\tilde{\mathcal{K}}_3(M_{a,b},\Delta_1,\Delta_2) &= \delta_{a,b}\{A_{a,b}\mathcal{K}(M_{a,b},\Delta_1,\Delta_2) \\
&\quad + (1-A_{a,b})\mathcal{K}(M_X,\Delta_1,\Delta_2) \\
&\quad + C_{a,b}\mathcal{K}_{\eta'}(M_{a,b},\Delta_1,\Delta_2)\} \\
&\quad + (1-\delta_{a,b})\{D^{(a)}_{a,b}\mathcal{K}(M_{a,a},\Delta_1,\Delta_2) \\
&\quad + D^{(b)}_{a,b}\mathcal{K}(M_{b,b},\Delta_1,\Delta_2) \\
&\quad + D^{(X)}_{a,b}\mathcal{K}(M_X,\Delta_1,\Delta_2)\},
\end{aligned} \tag{B13}$$

in the SU(6|3) theory ($N_f = 3$).

TABLE III. Coefficients for S_{ij} baryon wave-function renormalization, in Eq. (48), in the isospin limit.

a	u	s	u'	s'
$w'^{(2)}_{S_{du},a} + u'^{(2)}_{S_{du},a}$	$\frac{-1}{2}$	0	1	0
$\tilde{w}'^{(2)}_{S_{du},a} + \tilde{u}'^{(2)}_{S_{du},a}$	0	0	0	0
$w^{(2)}_{S_{du},a} + u^{(2)}_{S_{du},a}$	$\frac{1}{2}$	0	1	0
$\tilde{w}^{(2)}_{S_{du},a} + \tilde{u}^{(2)}_{S_{du},a}$	$\frac{-1}{2}$	0	0	0
$w'^{(3)}_{S_{du},a} + u'^{(3)}_{S_{du},a}$	$\frac{-1}{2}$	0	1	$\frac{1}{2}$
$\tilde{w}'^{(3)}_{S_{du},a} + \tilde{u}'^{(3)}_{S_{du},a}$	0	0	0	0
$w^{(3)}_{S_{du},a} + u^{(3)}_{S_{du},a}$	$\frac{1}{2}$	0	1	$\frac{1}{2}$
$\tilde{w}^{(3)}_{S_{du},a} + \tilde{u}^{(3)}_{S_{du},a}$	$\frac{-1}{3}$	0	0	0
$w'^{(3)}_{S_{su},a}$	0	$\frac{-1}{4}$	$\frac{1}{2}$	$\frac{1}{4}$
$\tilde{w}'^{(3)}_{S_{su},a}$	$\frac{-1}{12}$	0	0	0
$u'^{(3)}_{S_{su},a}$	$\frac{-1}{4}$	0	$\frac{1}{2}$	$\frac{1}{4}$
$\tilde{u}'^{(3)}_{S_{su},a}$	$\frac{1}{6}$	$\frac{-1}{12}$	0	0
$w^{(3)}_{S_{su},a}$	0	$\frac{1}{4}$	$\frac{1}{2}$	$\frac{1}{4}$
$\tilde{w}^{(3)}_{S_{su},a}$	$\frac{-1}{12}$	0	0	0
$u^{(3)}_{S_{su},a}$	$\frac{1}{4}$	0	$\frac{1}{2}$	$\frac{1}{4}$
$\tilde{u}^{(3)}_{S_{su},a}$	$\frac{-1}{6}$	$\frac{-1}{12}$	0	0
$w'^{(3)}_{S_{ss},a} + u'^{(3)}_{S_{ss},a}$	0	$\frac{-1}{2}$	1	$\frac{1}{2}$
$\tilde{w}'^{(3)}_{S_{ss},a} + \tilde{u}'^{(3)}_{S_{ss},a}$	0	0	0	0
$w^{(3)}_{S_{ss},a} + u^{(3)}_{S_{ss},a}$	0	$\frac{1}{2}$	1	$\frac{1}{2}$
$\tilde{w}^{(3)}_{S_{ss},a} + \tilde{u}^{(3)}_{S_{ss},a}$	0	$\frac{-1}{3}$	0	0

TABLE IV. Coefficients $x^{(N_f)}_{H_1,H_2}$ in Eq. (51), in the isospin limit.

a	u	s	u'	s'
$x^{(2)}_{T_{du},S_{dd},a}$	-1	0	-1	0
$x^{(3)}_{T_{du},S_{dd},a}$	-1	0	-1	$\frac{-1}{2}$
$x^{(3)}_{T_{su},S_{sd},a}$	-1	0	-1	$\frac{-1}{2}$
$x^{(3)}_{T_{du},S_{ds},a}$	$\frac{-1}{2}$	$\frac{-1}{2}$	-1	$\frac{-1}{2}$
$x^{(3)}_{T_{su},S_{ss},a}$	$\frac{-1}{2}$	$\frac{-1}{2}$	-1	$\frac{-1}{2}$
$x^{(2)}_{S_{du},S_{dd},a}$	$\frac{-1}{2}$	0	$\frac{-1}{2}$	0
$x^{(3)}_{S_{du},S_{dd},a}$	$\frac{-1}{2}$	0	$\frac{-1}{2}$	$\frac{-1}{4}$
$x^{(3)}_{S_{su},S_{sd},a}$	$\frac{-1}{2}$	0	$\frac{-1}{2}$	$\frac{-1}{4}$
$x^{(3)}_{S_{du},S_{ds},a}$	$\frac{-1}{4}$	$\frac{-1}{4}$	$\frac{-1}{2}$	$\frac{-1}{4}$
$x^{(3)}_{S_{su},S_{ss},a}$	$\frac{-1}{4}$	$\frac{-1}{4}$	$\frac{-1}{2}$	$\frac{-1}{4}$

TABLE V. Coefficients $x^{\prime(N_f)}_{H_1,H_2}$ in Eq. (51), in the isospin limit.

a	u	s	u'	s'
$x^{\prime(2)}_{S_{du},S_{dd},a}$	0	0	-1	0
$x^{\prime(3)}_{S_{du},S_{dd},a}$	0	0	-1	$\frac{-1}{2}$
$x^{\prime(3)}_{S_{su},S_{sd},a}$	0	0	-1	$\frac{-1}{2}$
$x^{\prime(3)}_{S_{du},S_{ds},a}$	$\frac{1}{2}$	$\frac{-1}{2}$	-1	$\frac{-1}{2}$
$x^{\prime(3)}_{S_{su},S_{ss},a}$	$\frac{1}{2}$	$\frac{-1}{2}$	-1	$\frac{-1}{2}$

TABLE VI. Coefficients $x^{\prime(N_f)}_{H_1,H_2}$ in Eq. (51), in the isospin limit.

a	u	s	u'	s'
$x^{\prime\prime(2)}_{T_{du},S_{dd},a}$	0	0	-1	0
$x^{\prime\prime(3)}_{T_{du},S_{dd},a}$	0	0	-1	$\frac{-1}{2}$
$x^{\prime\prime(3)}_{T_{su},S_{sd},a}$	0	0	-1	$\frac{-1}{2}$
$x^{\prime\prime(3)}_{T_{du},S_{ds},a}$	$\frac{-1}{2}$	$\frac{1}{2}$	-1	$\frac{-1}{2}$
$x^{\prime\prime(3)}_{T_{su},S_{ss},a}$	$\frac{-1}{2}$	$\frac{1}{2}$	-1	$\frac{-1}{2}$
$x^{\prime\prime(2)}_{S_{du},S_{dd},a}$	0	0	-1	0
$x^{\prime\prime(3)}_{S_{du},S_{dd},a}$	0	0	-1	$\frac{-1}{2}$
$x^{\prime\prime(3)}_{S_{su},S_{sd},a}$	0	0	-1	$\frac{-1}{2}$
$x^{\prime\prime(3)}_{S_{du},S_{ds},a}$	$\frac{-1}{2}$	$\frac{1}{2}$	-1	$\frac{-1}{2}$
$x^{\prime\prime(3)}_{S_{su},S_{ss},a}$	$\frac{-1}{2}$	$\frac{1}{2}$	-1	$\frac{-1}{2}$

APPENDIX C: COEFFICIENTS FOR WAVE-FUNCTION RENORMALIZATION

In this Appendix, we present the coefficients in Eqs. (47) and (48) relevant to the matrix elements investigated in this work. These coefficients are summarized in Tables I, II, and III. Because of isospin symmetry, it is not possible (or necessary) to distinguish between the w and u coefficients

TABLE VIII. Coefficients $\tilde{x}^{(N_f)}_{H_1,H_2}$ in Eq. (51). Because of the isospin symmetry, some of them cannot be distinguished from their $\tilde{y}^{(N_f)}_{H_1,H_2}$ counterparts. For such cases, we present $\tilde{x}^{(N_f)}_{H_1,H_2} + \tilde{y}^{(N_f)}_{H_1,H_2}$ in the table.

a	u	s	u'	s'
$\tilde{x}^{(2)}_{T_{du},S_{dd},a}$	$0-\tilde{y}^{(2)}_{T_{du},S_{dd}}$	0	0	0
$\tilde{x}^{(3)}_{T_{du},S_{dd},a}$	$0-\tilde{y}^{(3)}_{T_{du},S_{dd}}$	0	0	0
$\tilde{x}^{(3)}_{T_{su},S_{sd},a}$	0	$\frac{1}{6}$	0	0
$\tilde{x}^{(3)}_{T_{du},S_{ds},a}$	0	$0-\tilde{y}^{(3)}_{T_{du},S_{ds}}$	0	0
$\tilde{x}^{(3)}_{T_{su},S_{ss},a}$	$\frac{-1}{3}-\tilde{y}^{(3)}_{T_{su},S_{ss}}$	$\frac{1}{3}$	0	0
$\tilde{x}^{(2)}_{S_{du},S_{dd},a}$	$\frac{1}{2}-\tilde{y}^{(2)}_{S_{du},S_{dd}}$	0	0	0
$\tilde{x}^{(3)}_{S_{du},S_{dd},a}$	$\frac{1}{3}-\tilde{y}^{(3)}_{S_{du},S_{dd}}$	0	0	0
$\tilde{x}^{(3)}_{S_{su},S_{sd},a}$	$\frac{1}{6}$	$\frac{1}{12}$	0	0
$\tilde{x}^{(3)}_{S_{du},S_{ds},a}$	$\frac{1}{6}$	$\frac{1}{6}-\tilde{y}^{(3)}_{S_{du},S_{ds}}$	0	0
$\tilde{x}^{(3)}_{S_{su},S_{ss},a}$	$\frac{1}{6}-\tilde{y}^{(3)}_{S_{su},S_{ss}}$	$\frac{1}{6}$	0	0

TABLE IX. Coefficients $\tilde{x}^{\prime(N_f)}_{H_1,H_2}$ in Eq. (51). Because of the isospin symmetry, some of them cannot be distinguished from their $\tilde{y}^{\prime(N_f)}_{H_1,H_2}$ counterparts. For such cases, we present $\tilde{x}^{\prime(N_f)}_{H_1,H_2} + \tilde{y}^{\prime(N_f)}_{H_1,H_2}$ in the table.

a	u	s	u'	s'
$\tilde{x}^{\prime(2)}_{S_{du},S_{dd},a}$	$0-\tilde{y}^{\prime(2)}_{S_{du},S_{dd}}$	0	0	0
$\tilde{x}^{\prime(3)}_{S_{du},S_{dd},a}$	$0-\tilde{y}^{\prime(3)}_{S_{du},S_{dd}}$	0	0	0
$\tilde{x}^{\prime(3)}_{S_{su},S_{sd},a}$	0	$\frac{1}{6}$	0	0
$\tilde{x}^{\prime(3)}_{S_{du},S_{ds},a}$	0	$0-\tilde{y}^{\prime(3)}_{S_{du},S_{ds}}$	0	0
$\tilde{x}^{\prime(3)}_{S_{su},S_{ss},a}$	$\frac{-1}{3}-\tilde{y}^{\prime(3)}_{S_{su},S_{ss}}$	$\frac{1}{3}$	0	0

TABLE VII. Coefficients $\tilde{y}^{(N_f)}_{H_1,H_2}$, $\tilde{y}^{\prime(N_f)}_{H_1,H_2}$, and $\tilde{y}^{\prime\prime(N_f)}_{H_1,H_2}$ in Eqs. (49) and (51). Because of the isospin symmetry, some of these coefficients cannot be distinguished from their $\tilde{x}^{(N_f)}_{H_1,H_2}$ counterparts. For such cases, the values are denoted $+\tilde{x}$ in the table, and are presented together with the corresponding $\tilde{x}^{(N_f)}_{H_1,H_2}$.

$\tilde{y}^{(2)}_{B_u,B_d^*}$	$\tilde{y}^{(3)}_{B_u,B_d^*}$	$\tilde{y}^{(3)}_{B_u,B_s^*}$	$\tilde{y}^{(2)}_{T_{du},S_{dd}}$	$\tilde{y}^{(3)}_{T_{du},S_{dd}}$	$\tilde{y}^{(3)}_{T_{su},S_{sd}}$	$\tilde{y}^{(3)}_{T_{du},S_{ds}}$	$\tilde{y}^{(3)}_{T_{su},S_{ss}}$	$\tilde{y}^{(2)}_{S_{du},S_{dd}}$	$\tilde{y}^{(3)}_{S_{du},S_{dd}}$	$\tilde{y}^{(3)}_{S_{su},S_{sd}}$	$\tilde{y}^{(3)}_{S_{du},S_{ds}}$	$\tilde{y}^{(3)}_{S_{su},S_{ss}}$
-1	$\frac{-2}{3}$	$\frac{-2}{3}$	$+\tilde{x}$	$+\tilde{x}$	$\frac{-1}{6}$	$+\tilde{x}$	$+\tilde{x}$	$+\tilde{x}$	$+\tilde{x}$	$\frac{1}{12}$	$+\tilde{x}$	$+\tilde{x}$

$\tilde{y}^{\prime(2)}_{B_u,B_d^*}$	$\tilde{y}^{\prime(3)}_{B_u,B_d^*}$	$\tilde{y}^{\prime(3)}_{B_u,B_s^*}$	$\tilde{y}^{\prime(2)}_{S_{du},S_{dd}}$	$\tilde{y}^{\prime(3)}_{S_{du},S_{dd}}$	$\tilde{y}^{\prime(3)}_{S_{su},S_{sd}}$	$\tilde{y}^{\prime(3)}_{S_{du},S_{ds}}$	$\tilde{y}^{\prime(3)}_{S_{su},S_{ss}}$
$\frac{1}{2}$	$\frac{1}{3}$	$\frac{1}{3}$	$+\tilde{x}'$	$+\tilde{x}'$	$\frac{-1}{6}$	$+\tilde{x}'$	$+\tilde{x}'$

$\tilde{y}^{\prime\prime(2)}_{T_{du},S_{dd}}$	$\tilde{y}^{\prime\prime(3)}_{T_{du},S_{dd}}$	$\tilde{y}^{\prime\prime(3)}_{T_{su},S_{sd}}$	$\tilde{y}^{\prime\prime(3)}_{T_{du},S_{ds}}$	$\tilde{y}^{\prime\prime(3)}_{T_{su},S_{ss}}$	$\tilde{y}^{\prime\prime(2)}_{S_{du},S_{dd}}$	$\tilde{y}^{\prime\prime(3)}_{S_{du},S_{dd}}$	$\tilde{y}^{\prime\prime(3)}_{S_{su},S_{sd}}$	$\tilde{y}^{\prime\prime(3)}_{S_{du},S_{ds}}$	$\tilde{y}^{\prime\prime(3)}_{S_{su},S_{ss}}$
$+\tilde{x}''$	$+\tilde{x}''$	$\frac{1}{6}$	$+\tilde{x}''$	$+\tilde{x}''$	$+\tilde{x}''$	$+\tilde{x}''$	$\frac{-1}{6}$	$+\tilde{x}''$	$+\tilde{x}''$

TABLE X. Coefficients $\tilde{x}^{II(N_f)}_{H_1,H_2}$ in Eq. (51). Because of the isospin symmetry, some of them cannot be distinguished from their $\tilde{y}^{II(N_f)}_{H_1,H_2}$ counterparts. For such cases, we present $\tilde{x}^{II(N_f)}_{H_1,H_2} + \tilde{y}^{II(N_f)}_{H_1,H_2}$ in the table.

a	u	s	u'	s'
$\tilde{x}^{II(2)}_{T_{du},S_{dd},a}$	$0 - \tilde{y}^{II(2)}_{T_{du},S_{dd}}$	0	0	0
$\tilde{x}^{II(3)}_{T_{du},S_{dd},a}$	$0 - \tilde{y}^{II(3)}_{T_{du},S_{dd}}$	0	0	0
$\tilde{x}^{II(3)}_{T_{su},S_{sd},a}$	$\frac{-1}{3}$	$\frac{1}{6}$	0	0
$\tilde{x}^{II(3)}_{T_{du},S_{ds},a}$	0	$0 - \tilde{y}^{II(3)}_{T_{du},S_{ds}}$	0	0
$\tilde{x}^{II(3)}_{T_{su},S_{ss},a}$	$0 - \tilde{y}^{II(3)}_{T_{su},S_{ss}}$	0	0	0
$\tilde{x}^{II(2)}_{S_{du},S_{dd},a}$	$0 - \tilde{y}^{II(2)}_{S_{du},S_{dd}}$	0	0	0
$\tilde{x}^{II(3)}_{S_{du},S_{dd},a}$	$0 - \tilde{y}^{II(3)}_{S_{du},S_{dd}}$	0	0	0
$\tilde{x}^{II(3)}_{S_{su},S_{sd},a}$	0	$\frac{1}{6}$	0	0
$\tilde{x}^{II(3)}_{S_{du},S_{ds},a}$	$\frac{1}{3}$	$\frac{-1}{3} - \tilde{y}^{II(3)}_{S_{du},S_{ds}}$	0	0
$\tilde{x}^{II(3)}_{S_{su},S_{ss},a}$	$0 - \tilde{y}^{II(3)}_{S_{su},S_{ss}}$	0	0	0

for some of the hadrons in the current study. For such cases, we simply present $w + u$ in the tables.

APPENDIX D: COEFFICIENTS FOR THE SUNSET DIAGRAMS

In this Appendix, we present the coefficients in Eqs. (49) and (51) relevant to the matrix elements investigated in this work. Because of the isospin symmetry, it is impossible to distinguish between some $\tilde{y}$ coefficients and their $\tilde{x}$ counterparts. For such cases, we put the symbol $+\tilde{x}$ in Table VII, and then present $\tilde{x} + \tilde{y}$ in Tables VIII, IX, and X in the form that $\tilde{x}$ is written as (number-$\tilde{y}$).

[1] G. Burdman and J. F. Donoghue, Phys. Lett. B **280**, 287 (1992).
[2] M. B. Wise, Phys. Rev. D **45**, R2188 (1992).
[3] T.-M. Yan *et al.*, Phys. Rev. D **46**, 1148 (1992); **55**, 5851 (E) (1997).
[4] P. L. Cho, Phys. Lett. B **285**, 145 (1992).
[5] P. L. Cho, Nucl. Phys. **B396**, 183 (1993); **B421**, 683(E) (1994).
[6] C. W. Bernard and M. F. L. Golterman, Phys. Rev. D **49**, 486 (1994).
[7] F. Bernardoni, P. Hernandez, and S. Necco, J. High Energy Phys. 01 (2010) 070.
[8] R. A. Briceno, arXiv:1108.0120.
[9] D. Arndt and C.-J. D. Lin, Phys. Rev. D **70**, 014503 (2004).
[10] W. Detmold and C.-J. D. Lin, Phys. Rev. D **76**, 014501 (2007).
[11] G. Colangelo, A. Fuhrer, and S. Lanz, Phys. Rev. D **82**, 034506 (2010).
[12] G. de Divitiis *et al.* (UKQCD Collaboration), J. High Energy Phys. 10 (1998) 010.
[13] A. Abada, D. Becirevic, P. Boucaud, G. Herdoiza, J. Leroy *et al.*, J. High Energy Phys. 02 (2004) 016.
[14] H. Ohki, H. Matsufuru, and T. Onogi, Phys. Rev. D **77**, 094509 (2008).
[15] D. Becirevic, B. Blossier, E. Chang, and B. Haas, Phys. Lett. B **679**, 231 (2009).
[16] J. Bulava, M. Donnellan, and R. Sommer (ALPHA Collaboration), Proc. Sci., LAT2010 (2010) 303 [arXiv:1011.4393].
[17] J. Bulava, M. Donnellan, and R. Sommer, arXiv:1108.3774.
[18] C. W. Bernard and M. F. L. Golterman, Phys. Rev. D **53**, 476 (1996).
[19] S. R. Sharpe and N. Shoresh, Phys. Rev. D **64**, 114510 (2001).
[20] S. R. Sharpe and N. Shoresh, Phys. Rev. D **62**, 094503 (2000).
[21] S. R. Sharpe and Y. Zhang, Phys. Rev. D **53**, 5125 (1996).
[22] M. J. Savage, Phys. Rev. D **65**, 034014 (2002).
[23] C. G. Boyd and B. Grinstein, Nucl. Phys. **B442**, 205 (1995).
[24] K. Nakamura *et al.* (Particle Data Group), J. Phys. G **37**, 075021 (2010).
[25] D. Arndt, S. R. Beane, and M. J. Savage, Nucl. Phys. **A726**, 339 (2003).
[26] T. Aaltonen *et al.* (CDF Collaboration), Phys. Rev. Lett. **99**, 202001 (2007).
[27] I. W. Stewart, Nucl. Phys. **B529**, 62 (1998).
[28] J. Gasser and H. Leutwyler, Nucl. Phys. **B250**, 465 (1985).

[29] B. C. Tiburzi and A. Walker-Loud, Nucl. Phys. **A764**, 274 (2006).
[30] A. Walker-Loud, Ph.D. Thesis, 2006, arXiv:hep-lat/0608010.
[31] L. Lellouch and M. Lüscher, Commun. Math. Phys. **219**, 31 (2001).
[32] V. Bernard, U.-G. Meissner, and A. Rusetsky, Nucl. Phys. **B788**, 1 (2008).
[33] W. Detmold, C.-J. D. Lin, and S. Meinel (unpublished).
[34] S. R. Sharpe, Phys. Rev. D **46**, 3146 (1992).
[35] B. C. Tiburzi, Phys. Rev. D **71**, 034501 (2005).
[36] H.-Y. Cheng, C.-Y. Cheung, G.-L. Lin, Y. Lin, T.-M. Yan *et al.*, Phys. Rev. D **49**, 5857 (1994).
[37] W. Detmold and C.-J. D. Lin, Phys. Rev. D **71**, 054510 (2005).
[38] S. R. Beane, Phys. Rev. D **70**, 034507 (2004).